

On the inconsistency of [C/Fe] abundances and the fractions of carbon-enhanced metal-poor stars among various stellar surveys

Anke Arentsen,^{1*} Vinicius M. Placco,² Young Sun Lee,³ David S. Aguado,^{4,5} Nicolas F. Martin,^{1,6} Else Starkenburg,⁷ Jinmi Yoon^{8,9}

¹ *Université de Strasbourg, CNRS, Observatoire astronomique de Strasbourg, UMR 7550, F-67000 Strasbourg, France*

² *NSF's NOIRLab, 950 N. Cherry Ave., Tucson, AZ 85719, USA*

³ *Department of Astronomy and Space Science, Chungnam National University, Daejeon 34134, Republic of Korea*

⁴ *Dipartimento di Fisica e Astrofisica, Università degli Studi di Firenze, via G. Sansone 1, I-50019 Sesto Fiorentino, Italy*

⁵ *INAF/Osservatorio Astrofisico di Arcetri, Largo E. Fermi 5, I-50125 Firenze, Italy*

⁶ *Max-Planck-Institut für Astronomie, Königstuhl 17, D-69117 Heidelberg, Germany*

⁷ *Kapteyn Astronomical Institute, University of Groningen, Postbus 800, 9700 AV, Groningen, the Netherlands*

⁸ *Space Telescope Science Institute, 3700 San Martin Dr., Baltimore, MD 21218, USA*

⁹ *Joint Institute for Nuclear Astrophysics – Center for the Evolution of the Elements (JINA-CEE), USA*

Accepted 2022 July 20. Received 2022 July 19, in original form 2022 June 8

ABSTRACT

Carbon-enhanced metal-poor (CEMP) stars are a unique resource for Galactic archaeology because they probe the properties of the First Stars, early chemical evolution and binary interactions at very low metallicity. Comparing the fractions and properties of CEMP stars in different Galactic environments can provide us with unique insights into the formation and evolution of the Milky Way halo and its building blocks. In this work, we investigate whether directly comparing fractions of CEMP stars from different literature samples of very metal-poor ($[\text{Fe}/\text{H}] < -2.0$) stars is valid. We compiled published CEMP fractions and samples of Galactic halo stars from the past 25 years, and find that they are not all consistent with each other. Focusing on giant stars, we find significant differences between various surveys when comparing their trends of $[\text{Fe}/\text{H}]$ versus $[\text{C}/\text{Fe}]$ and their distributions of CEMP stars. To test the role of the analysis pipelines for low-resolution spectroscopic samples, we re-analysed giant stars from various surveys with the SSPP and FERRE pipelines. We found systematic differences in $[\text{C}/\text{Fe}]$ of $\sim 0.1 - 0.4$ dex, partly independent of degeneracies with the stellar atmospheric parameters. These systematics are likely due to the different pipeline approaches, different assumptions in the employed synthetic grids, and/or the comparison of different evolutionary phases. We conclude that current biases in (the analysis of) very metal-poor samples limit the conclusions one can draw from comparing different surveys. We provide some recommendations and suggestions that will hopefully aid the community to unlock the full potential of CEMP stars for Galactic archaeology.

Key words: stars: chemically peculiar – stars: Population II – stars: abundances – techniques: spectroscopic – methods: data analysis

1 INTRODUCTION

Very metal-poor stars are useful probes for Galactic archaeology, since they are old and contain key information about the early Universe. However, they are rare and often dedicated or very large surveys are needed to find them. A surprise in the early HK prism survey of metal-poor stars (Beers et al. 1992, hereafter BPS) was that many very metal-poor stars appeared to have exceptionally strong carbon features. Norris et al. (1997) calculate the fraction and find that $\sim 10\%$ of the BPS stars have ‘stronger than normal G-band strengths’ – broken down by metallicity these fractions are 14%, 4% and 4% for $[\text{Fe}/\text{H}]$ ¹

< -2.5 , $-2.5 < [\text{Fe}/\text{H}] < -1.5$ and $-1.5 < [\text{Fe}/\text{H}] < -0.5$, respectively. They also point out that Luck & Bond (1991) find 1% of carbon-rich stars (CH stars) among metal-poor disk stars (with average $[\text{Fe}/\text{H}] = -0.4$), and conclude that the fraction of carbon-rich stars increases with decreasing metallicity. These stars were dubbed carbon-enhanced metal-poor (CEMP) stars by Beers & Christlieb (2005), who set the criterion for a star to be CEMP at $[\text{C}/\text{Fe}] > +1.0$ and $[\text{Fe}/\text{H}] < -1.0$. Since then, many CEMP stars were found in (metal-poor) surveys such as the Hamburg/ESO (HES) survey (Christlieb et al. 2008) and the Sloan Digital Sky Survey (SDSS, York et al. 2000) (e.g. Carollo et al. 2012; Lee et al. 2013). Reported CEMP fractions were between 10 – 30% for very metal-poor (VMP, $[\text{Fe}/\text{H}] < -2.0$) stars (e.g. Lucatello et al. 2006; Lee et al. 2013; Placco et al. 2014), and typically increase with decreasing metallicity.

* E-mail: anke.arentsen@astro.unistra.fr

¹ $[\text{X}/\text{Y}] = \log(N_{\text{X}}/N_{\text{Y}})_{*} - \log(N_{\text{X}}/N_{\text{Y}})_{\odot}$, where the asterisk subscript refers to the considered star, and N is the number density.

Many CEMP stars have been studied in detail in recent years. The two most common types of CEMP stars are CEMP-s stars, which have an excess of slow neutron-capture (s-process) elements as well as a high carbon abundance, and CEMP-no stars, which do not show the s-process enhanced signature but do have a high carbon abundance. There are also CEMP-r, CEMP-r/s stars and CEMP-i stars, enhanced with rapid and/or intermediate neutron-capture processes, which are more rare and will not be considered in this work. The CEMP-s stars are common at $[\text{Fe}/\text{H}] > -3.0$ and are thought to form through binary interaction with a former asymptotic giant branch (AGB) companion. This is supported by their chemical abundance patterns and a high binary fraction (e.g. [Lucatello et al. 2005](#); [Bisterzo et al. 2010](#); [Abate et al. 2015](#); [Hansen et al. 2016b](#)). The CEMP-no stars, on the other hand, are dominant at $[\text{Fe}/\text{H}] < -3.0$ and are thought to have been born with their high carbon abundance, from gas polluted by the first generations of stars (for a review on extremely metal-poor stars including CEMP-no stars, see [Frebel & Norris 2015](#)). Their binary fraction is much lower than that of CEMP-s stars ([Norris et al. 2013b](#); [Starkenburg et al. 2014](#); [Hansen et al. 2016a](#)), although it appears to be higher than that of normal metal-poor stars ([Arentsen et al. 2019](#)). There are several mechanisms related to the First Stars that could cause high yields of carbon, such as their explosion as mixing-and-fallback (faint) supernovae (e.g. [Umeda & Nomoto 2003](#); [Nomoto et al. 2013](#); [Tominaga et al. 2014](#)) and/or their exceptionally high rotation rates (e.g. [Chiappini et al. 2006](#); [Meynet et al. 2006](#); [Heger & Woosley 2010](#)).

Knowing the fraction of CEMP stars relative to carbon-normal stars, especially for CEMP-s and CEMP-no stars separately, is important for our interpretation of populations of metal-poor stars. The fraction of CEMP-s stars teaches us about the binary fraction of low-metallicity stars in a population, about the properties of those binary systems and about the way they interact with their (former) AGB companions. The fraction of CEMP-no stars can shed light on the importance of peculiar processes in the First Stars and on the rate of chemical evolution in the birth environments of extremely metal-poor stars in the early Universe. Differences in the fractions of CEMP stars between Galactic environments can provide us with valuable clues about the different conditions in structures in the early Universe.

Almost all samples of low-metallicity stars contain high numbers of CEMP stars, but the discussion is still ongoing what exactly the fraction of CEMP stars is as a function of metallicity, how it changes for the different classes of CEMP stars and different stellar evolutionary phases ([Beers & Christlieb 2005](#); [Cohen et al. 2005](#); [Frebel et al. 2006](#); [Lucatello et al. 2006](#); [Aoki et al. 2007](#); [Carollo et al. 2012](#); [Lee et al. 2013](#); [Yong et al. 2013](#); [Lee et al. 2014](#); [Placco et al. 2014](#); [Beers et al. 2017](#); [Yoon et al. 2018](#); [Placco et al. 2018, 2019](#); [Limberg et al. 2021](#); [Whitten et al. 2021](#); [Shank et al. 2021](#)), and how it may be different in different Galactic environments, such as different regions of the halo ([Frebel et al. 2006](#); [Carollo et al. 2012, 2014](#); [Lee et al. 2017](#); [Beers et al. 2017](#); [Lee et al. 2019](#); [Yoon et al. 2018](#)), dwarf galaxies (e.g. [Starkenburg et al. 2013](#); [Salvadori et al. 2015](#); [Chiti et al. 2018](#); [Yoon et al. 2019](#); [Ji et al. 2020](#)), globular clusters ([D'Orazi et al. 2010](#)), stellar streams ([Aguado et al. 2021](#)) and the Galactic bulge ([Howes et al. 2016](#); [Arentsen et al. 2021](#)). There are many uncertainties in determining the CEMP fraction, e.g. due to selection effects in samples of metal-poor stars, challenges in measuring stellar parameters and carbon abundances, and difficulties with the classification of different types of CEMP stars. Additionally, comparisons between literature fractions are sometimes hampered by the adoption of different CEMP star definitions and whether or not

corrections for the evolutionary stage of the stars have been taken into account.

Ideally, when comparing different VMP/CEMP samples, stars of similar evolutionary phases should be used because they have experienced similar evolutionary effects. Additionally, their spectral analysis will suffer from similar systematics due to e.g. the assumption of local thermodynamic equilibrium (LTE) and calculations in one dimension (1D) for the computation of synthetic model spectra. In environments other than the Galactic halo, such as the Galactic bulge, dwarf galaxies, globular clusters or stellar streams, VMP samples typically consist of giant stars because these are bright. It is therefore important to study the CEMP fraction among giant stars, if we want to interpret the CEMP fraction in different environments. This is the focus of this paper.

Giants are cool ($T_{\text{eff}} < 5700$ K) and have clear carbon features, which can easily be detected in low-resolution spectroscopy. Their CEMP fraction, however, can be challenging to interpret. Giants can suffer from evolutionary effects that change their surface $[\text{C}/\text{Fe}]$, which needs to be corrected for, and samples could be a mix of red giant branch (RGB) and early AGB stars, which have experienced different evolutionary effects. It is also not trivial to analyse spectra of cool, carbon-rich stars, which are dominated by molecular bands (e.g. [Beers et al. 1999](#); [Rossi et al. 2005](#); [Goswami et al. 2006](#); [Yoon et al. 2020](#)), and finally, their photometry is also affected due to the large carbon features, leading to sample selection effects.

We review the various reported CEMP fractions in the literature in Section 2, and discuss issues in comparing them with each other. In Section 3, we compare two pipelines for low-resolution spectroscopic analysis of VMP giants and discuss implications for some previously derived CEMP fractions. We summarise our results in Section 4, concluding that there is still more work to be done before we can safely compare and interpret CEMP fractions of giant stars.

2 LITERATURE CEMP FRACTIONS

There are many reported values of CEMP fractions among metal-poor halo stars in the literature. In this section, we discuss various reports throughout the years, separated into low ($R \lesssim 2500$) and high ($R \gtrsim 15000$) resolution spectroscopic samples. An overview is presented in Table 1 (not all of those will be mentioned in the text, and the compilation may also not be exhaustive). For giant stars, the different cumulative CEMP fractions are shown in Figure 1, summing all stars below a given metallicity. We also discuss the relative occurrence of CEMP-s and CEMP-no stars in various samples. We end this section with a summary and a discussion of the literature comparisons.

2.1 Low/medium resolution samples

2.1.1 Early estimates

The first large spectroscopic samples of very metal-poor (VMP, $[\text{Fe}/\text{H}] < -2.0$) stars were built by following up exciting, metal-poor looking candidates from objective prism efforts such as the HK and HES surveys. In the review by [Beers & Christlieb \(2005\)](#), a carbon-enhanced ($[\text{C}/\text{Fe}] > +1.0$) fraction of $\sim 20\%$ among VMP stars is quoted, determined from ‘moderate-resolution follow-up spectra’ of objective prism surveys (but no further details are provided). Another early number which is regularly cited is 25% by [Marsteller et al. \(2005\)](#), but again no details are given as to how this number was derived.

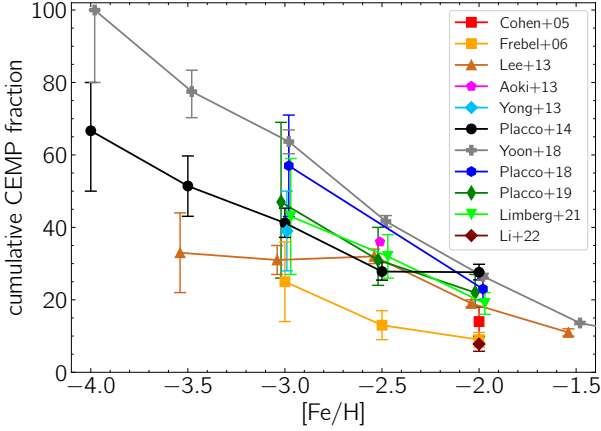


Figure 1. Cumulative fraction of CEMP stars as function of metallicity for samples of giant stars (see Table 1), including all sub-types of CEMP stars. Follow-up samples from narrow-band photometric surveys are not included. The $[C/Fe] > +0.7$ CEMP definition was used in all samples, except those of Cohen et al. (2005) and Frebel et al. (2006), who used $[C/Fe] > +1.0$. These are plotted with square symbols. Evolutionary corrections (following either Aoki et al. 2007 or Placco et al. 2014) have been taken into account in all cases, except for Cohen et al. (2005), Frebel et al. (2006) and Lee et al. (2013). Small offsets in $[Fe/H]$ have been applied to avoid overlap between points.

Cohen et al. (2005) analyse a sample of HES stars with high-resolution spectroscopy and discuss issues with the Beers et al. (1999) metallicity and carbon abundance scale for cool stars used in previous HES and HK medium-resolution analyses – if they correct for those effects they find a slightly lower fraction of CEMP stars of $14\% \pm 4\%$. Frebel et al. (2006) use an updated calibration for the derivation of $[C/Fe]$ from medium-resolution spectra (Rossi et al. 2005), and find a CEMP fraction of $9\% \pm 2\%$ in a HES medium-resolution follow-up VMP sample of giants. They comment that this is similar to the fraction by Cohen et al. (2005), although slightly lower, possibly due to limitations in the analysis for stars with very strong carbon bands. They also found that the CEMP fraction rises to $13\% \pm 4\%$ and $25\% \pm 11\%$ for $[Fe/H] < -2.5$ and < -3.0 , respectively, and that the CEMP fraction appears to be larger for stars further away from the Galactic disc.

2.1.2 Change in definitions

We note that Aoki et al. (2007) proposed a new definition of CEMP stars, lowering the CEMP threshold to $[C/Fe] = +0.7$ instead of $+1.0$ because that appeared to be a more natural division between carbon-normal and carbon-rich stars. They also added a dependence of the threshold on the evolutionary status/luminosity of a star, which is important for giants since the surface carbon abundance of evolved stars decreases during their ascent on the RGB. This was further studied by Placco et al. (2014), who derived $[C/Fe]$ corrections based on the evolutionary stage of a star and its metallicity and measured carbon abundance. Some have argued that the $[C/Fe] = +0.7$ threshold is not optimal since it may lead to spurious classifications (Bonifacio et al. 2015), but it has been widely adopted. All fractions described above considered stars with $[C/Fe] > +1.0$ to be CEMP and did not take into account evolutionary effects. The following CEMP fractions in the remainder of this section assume a CEMP definition of

$[C/Fe] > +0.7$, unless otherwise specified. They are inhomogeneous in whether or not they took into account any evolutionary corrections.

2.1.3 SDSS

Other than employing dedicated metal-poor surveys such as HK and HES to determine CEMP fractions, one can use large surveys that do not directly target very metal-poor stars. These have the advantage that they are expected to be less biased in their targeting (apart from e.g. cuts in brightness and colour), whereas the HK and HES samples for example could be biased by human choices in the selection for follow-up.

Carollo et al. (2012) analyse $\sim 30\,000$ calibration stars in SDSS/SEGUE (a mixture of dwarf, turn-off and subgiant/giant stars) using the SEGUE Stellar Parameter Pipeline (SSPP, Lee et al. 2008a,b) and report a CEMP fraction of 12% among VMP stars (with $[Fe/H] < -2.0$). The fraction decreases to 8% for $[Fe/H] < -1.5$, and increases to 20% for stars with $[Fe/H] < -2.5$. They also find trends between the CEMP fraction and the height above the disc, as in Frebel et al. (2006).

Lee et al. (2013) developed a method for determining $[C/Fe]$ and implemented it into the SSPP, and derive carbon abundances for a much larger sample of several hundred thousand SDSS stars (of all metallicities, not just VMP stars). They combine their sample with high-resolution literature samples for the extremely metal-poor stars ($[Fe/H] < -3.0$), and find CEMP fractions consistent with Carollo et al. (2012) to within 1%. If they adopt a CEMP definition of $[C/Fe] > +1.0$, their fractions are consistent with those from Frebel et al. (2006) as well. Lee et al. also report CEMP fractions for extremely metal-poor stars, which are further increasing to $28\% \pm 3\%$ for $[Fe/H] < -3.0$ and $43\% \pm 11\%$ for $[Fe/H] < -3.5$. The authors find that there is a large discrepancy between CEMP fractions determined from giants and turn-off stars (they also test dwarfs, but most VMP stars are in the other categories) – the cumulative fractions for $[Fe/H] < -2.0$, -2.5 and -3.0 are $\sim 2 - 3$ times higher among giants compared to the hotter turn-off stars (the giant fractions are 19%, 32% and 31%, respectively). They interpret this as a result of the difficulty to measure carbon abundances for hot stars (e.g., turn-off stars) – at higher temperatures, the CH G-band can only be detected for stars with very high carbon abundances, and stars with moderate carbon-enhancement would be missed. There is also a systematic effect with metallicity, as it is more difficult to detect the G-band for more metal-poor stars. No evolutionary corrections were applied in either Carollo et al. (2012) or Lee et al. (2013).

2.1.4 Recent estimates

In recent years, CEMP fractions were determined for many more large samples of metal-poor stars with low-resolution spectroscopy. All stellar parameter and carbon abundance determinations for these samples were performed using an adapted version of the SSPP for non-SDSS/SEGUE spectra (called n-SSPP), except for samples from the *Pristine* survey (which will be discussed later). For example Beers et al. (2017), using on a mixed sample of dwarfs, turn-off stars and giants selected from HES, found CEMP fractions largely consistent with previous estimates from SDSS. Other examples are Yoon et al. (2018) using stars from the AAOmega Evolution of Galactic Structure (AEGIS) survey (a follow-up survey based on SkyMapper data, Wolf et al. 2018), Placco et al. (2018) for metal-poor stars selected from the RAdial Velocity Experiment (RAVE, Steinmetz et al. 2006), and Placco et al. (2019) and Limberg et al. (2021) for stars selected

from the Best & Brightest (B&B, [Schlaufman & Casey 2014](#)) survey. All of these followed up mostly (sub)giant stars (due to selection biases in the original surveys), and typically find CEMP fractions higher than any other reported fractions in the literature based on low-resolution spectroscopy. For example, [Yoon et al. \(2018\)](#) find CEMP fractions of 27%, 42% and 64% for $[\text{Fe}/\text{H}] < -2.0$, -2.5 and -3.0 in the AEGIS survey. The higher fraction in these recent samples might be because they do not contain hot stars and therefore they miss fewer moderately carbon-rich objects, and also because the [Placco et al. \(2014\)](#) corrections for evolutionary effects on $[\text{C}/\text{Fe}]$ were applied in all these works. However, we will show in Section 3 that there might be another reason for the high CEMP fractions in these samples.

A lot of work has also been done to identify and specifically search for CEMP stars, for example using colours, prism-spectroscopy or infrared spectroscopy (e.g. [Beers et al. 1992](#); [Christlieb et al. 2001](#); [Placco et al. 2010, 2011](#); [Kielty et al. 2017](#)). Such samples cannot be used to determine the fraction of CEMP stars, but are still valuable sources for high-resolution spectroscopic follow-up.

2.1.5 CEMP-no vs. CEMP-s

Low-resolution samples typically cannot distinguish between CEMP-no stars and CEMP-s stars based on their neutron-capture abundances, because of the intrinsic weakness of the absorption features. However, fortunately CEMP stars of different types not only differ in their neutron-capture abundances, but they also have different distributions in their metallicity and carbon abundances (e.g. [Spite et al. 2013](#); [Bonifacio et al. 2015](#); [Yoon et al. 2016](#)). CEMP-s stars tend to have $[\text{Fe}/\text{H}] > -3.5$ and absolute carbon abundance² $A(\text{C}) > 7.0$ (called Group I stars by [Yoon et al. 2016](#)), while CEMP-no stars occupy the regions with lower $[\text{Fe}/\text{H}]$ and/or $A(\text{C})$ ([Yoon et al. 2016](#) identify two different regions, which they call Group II and III). [Yoon et al. \(2018\)](#) present separate CEMP frequencies for Group I (or CEMP-s) and Group II and III (CEMP-no) for their AEGIS low-resolution spectroscopic sample. For $[\text{Fe}/\text{H}] < -2.0$, they find Group II+III and Group I fractions of 17% and 10%, respectively. The fraction of Group II+III CEMP stars among stars with $[\text{Fe}/\text{H}] < -2.5$, -3.0 and -3.5 rises to 35%, 54% and 68%, respectively, while the Group I fraction stays relatively constant with 6%, 10% and 10%, respectively.

2.2 High resolution samples

2.2.1 [Lucatello et al. \(2006\)](#)

After the first confirmations of very metal-poor stars with low/medium-resolution spectroscopy, extensive follow-up campaigns with high-resolution spectroscopy started. Abundances from high-resolution spectroscopy are more precise and extensive, a clear advantage over using low-resolution samples for the determination of CEMP fractions, although the sample sizes are typically smaller. From high-resolution spectroscopic follow-up of 270 very metal-poor stars from the HES R-process enhanced star (HERES, [Barklem et al. 2005](#)) survey, [Lucatello et al. \(2006\)](#) derive a CEMP fraction ($[\text{C}/\text{Fe}] > +1.0$) of $21\% \pm 2\%$ for $[\text{Fe}/\text{H}] < -2.0$. They find that the fraction does not change when considering only unevolved stars. The CEMP fraction in their sample increases slightly, to $24\% \pm 3\%$, when adopting the [Aoki et al. \(2007\)](#) definition. They do not report

fractions for different metallicity ranges, although the CEMP fraction for stars with $[\text{Fe}/\text{H}] < -3.0$ appears much smaller than the fraction for $[\text{Fe}/\text{H}] < -2.0$ from their Figure 1.

[Lucatello et al. \(2006\)](#) discuss that the criteria to select HERES stars from the HES medium-resolution spectroscopy sample were specifically set to minimise biases in, for example, carbon abundance, and therefore assumed that their derived CEMP fraction was not biased. However, it was later recognised that some other high-resolution HES samples did have biases towards C-rich stars (see e.g. [Cohen et al. 2013](#)). This was due to systematics in the early analysis of the medium-resolution spectra, producing biased metallicities and carbon abundances.

2.2.2 [Yong et al. \(2013\)](#)

[Yong et al. \(2013\)](#) report a CEMP fraction focusing especially on the extremely metal-poor regime ($[\text{Fe}/\text{H}] < -3.0$). They re-analyse 152 stars with high-resolution spectroscopy from the literature and combine it with a HES follow-up sample of 38 stars from their earlier work ([Norris et al. 2013a](#)). Most of the literature stars originate from follow-up of the HK and HES surveys, and there is also a small number from other sources such as high proper motion surveys. Detailed studies of the HES metallicity distribution function (MDF) completeness were presented in [Schörck et al. \(2009\)](#) and [Li et al. \(2010\)](#), who concluded that the HES selection is complete for $[\text{Fe}/\text{H}] < -3.0$. [Yong et al. \(2013\)](#) carefully propagate this information (for both HK and HES stars) to their sample, but little is known about the selection function of the remainder of the literature stars.

From the 69 stars in their sample with $[\text{Fe}/\text{H}] < -3.0$, they report a CEMP fraction of $32\% \pm 8\%$ (adopting the [Aoki et al. 2007](#) definition). They find that the CEMP fraction appears to be higher for dwarfs, which they interpret as the result of the difficulty to measure carbon abundances in these hotter stars – several have upper limits on the carbon abundance above $[\text{C}/\text{Fe}] = +0.7$, and these are not taken into account in the fraction computation. [Yong et al. \(2013\)](#) do not report CEMP fractions for $[\text{Fe}/\text{H}] > -3.0$ as they were worried that there may possibly be a bias towards CEMP stars for these metallicities in the sample. For example such a bias could be due to the [Norris et al. \(2013a\)](#) part of the sample for which the strategy included observing ‘objects with prominent G bands in their medium-resolution spectra’ for the more metal-rich candidates.

2.2.3 [Placco et al. \(2014\)](#)

The CEMP fraction published by [Placco et al. \(2014, hereafter P14\)](#) is based on a compilation from the high-resolution literature as well, combining stars from the SAGA database ([Suda et al. 2008](#)) and the [Frebel \(2010\)](#) compilation. The final sample consists of 505 stars with $[\text{Fe}/\text{H}] < -2.0$ and a measurement of $[\text{C}/\text{Fe}]$ (no stars with only upper limits were included, which could introduce some biases). A significant difference with previous works is the use of individual evolutionary carbon corrections, based on stellar evolution models and using the $\log g$, $[\text{Fe}/\text{H}]$ and measured $[\text{C}/\text{Fe}]$ of each star. This allows for fairer CEMP fraction estimates from giant stars. P14 assume that their literature sample is not biased towards or against CEMP stars. The contributions to the literature come from many different sources, which all have different selection effects that may cancel each other out, but this is not necessarily true.

The overall CEMP fractions that they find are 33%, 34%, 48% and 60% for $[\text{Fe}/\text{H}] < -2.0$, -2.5 , -3.0 and -3.5 , respectively (using the CEMP definition of $[\text{C}/\text{Fe}] > +0.7$). This is higher than

² $A(\text{C}) = \log \epsilon(\text{C}) = \log(N_{\text{C}}/N_{\text{H}}) + 12$

all previous estimates (although similar to some of the more recent low-resolution estimates). It is expected to be somewhat higher due to the correction for evolutionary effects, but there may also be certain selection effects which are particularly troublesome for warmer stars (as discussed in multiple previous works). Re-calculating the numbers for only the giants ($T_{\text{eff}} < 5700$ K and $\log g < 3.8$) in the P14 sample, the fractions go down to 28%, 29%, 41% and 51% for $[\text{Fe}/\text{H}] < -2.0, -2.5, -3.0$ and -3.5 , respectively. This brings them somewhat closer to previous CEMP fractions. P14 also compute separate fractions for CEMP-no and CEMP-s stars. The fraction of CEMP-s stars decreases with decreasing $[\text{Fe}/\text{H}]$ from 13% to 10% to 5% to 0% for $[\text{Fe}/\text{H}] < -2.0, -2.5, -3.0, -3.5$, respectively, whereas the fraction of CEMP-no stars increases with decreasing metallicity: 20%, 24%, 43% and 60%.

2.2.4 SkyMapper

In recent years, many new metal-poor stars are being discovered in dedicated narrow-band photometric surveys. The SkyMapper survey in the Southern hemisphere employs the narrow-band v filter which includes the Ca H&K lines, and is therefore metallicity-sensitive (Keller et al. 2007). The CEMP fraction in the high-resolution follow-up SkyMapper sample of Yong et al. (2021) is 67% (6/9) for $[\text{Fe}/\text{H}] < -3.5$, 29% (19/66) for $[\text{Fe}/\text{H}] < -3.0$ and 20% (19/93) for $[\text{Fe}/\text{H}] < -2.5$, after P14 carbon-corrections, assuming a CEMP definition of $[\text{C}/\text{Fe}] > +0.7$ and excluding stars with upper limits on $[\text{C}/\text{Fe}]$. For $[\text{Fe}/\text{H}] < -2.5$ and -3.0 this is lower than the 34% and 48% reported by P14 for $[\text{Fe}/\text{H}] < -3.0$ and < -3.5 , respectively. The CEMP stars that are present in the sample all have relatively low $[\text{C}/\text{Fe}]$ ($\lesssim 1.5$), and almost none of them have $[\text{Fe}/\text{H}] > -3.0$. These lower frequencies of CEMP stars (and the lack of very carbon-rich CEMP stars) are interpreted as the result of photometric selection effects. The flux in the metallicity-sensitive v filter is affected by large molecular features for carbon-rich stars, making them look more metal-rich, hence creating a bias against selecting such stars for VMP follow-up (see e.g. Da Costa et al. 2019; Chiti et al. 2020).

The Extremely Metal-poor Bulge stars with AAOmega (EM-BLA) survey (Howes et al. 2014, 2015, 2016) is the follow-up of SkyMapper in the inner regions of the Milky Way. They selected targets for high-resolution spectroscopic follow-up from a large sample of low-resolution spectroscopic SkyMapper follow-up observations with the Anglo Australian Telescope (AAT). Out of 33 very metal-poor stars in their high-resolution sample, they found only one to be clearly carbon-enhanced (with $[\text{C}/\text{Fe}] > +1.0$). After correcting for evolutionary effects, there are five additional CEMP stars with $+0.7 < [\text{C}/\text{Fe}] < +1.0$, and the derived CEMP fractions are 44%, 18% and 20% for $[\text{Fe}/\text{H}] < -3.0, -2.5$ and -2.0 , respectively (Arentsen et al. 2021). Howes et al. (2016) discuss the possibility that the low frequency of CEMP stars in the bulge could hint at differences in the early chemical evolution between the inner Galaxy and the more distant halo, but also recognise that selection effects could be playing a role in the photometric SkyMapper selection.

2.2.5 LAMOST: Li et al. (2022)

Recently, a large high-resolution spectroscopic follow-up sample of VMP stars in LAMOST³ (Large sky Area Multi-Object fiber Spectroscopic Telescope) has been published by Li et al. (2022), with carbon abundances for 281 stars. They find very different CEMP fractions

for giants and turn-off stars in their sample, 7.8% and 31%, respectively, adopting $[\text{C}/\text{Fe}] > +0.7$ for CEMP stars. The turn-off CEMP fraction decreases to 22% when counting all stars with $[\text{C}/\text{Fe}]$ upper limits as carbon-normal, and to 11% when adopting $[\text{C}/\text{Fe}] > +1.0$ as CEMP definition. The difference in CEMP fractions between giants and turn-off stars is most striking for the CEMP-s stars, but also visible for CEMP-no stars. The authors suggest that this may be related to non-effective mixing during the turn-off phase, resulting in higher carbon abundances in turn-off stars than in giants.

The CEMP fraction in the Li et al. (2022) sample is much lower for VMP giants than in other literature samples, whereas for turn-off stars it is similar to previous estimates. The target selection was based on promising very metal-poor candidates from the analysis of the low-resolution LAMOST spectra (Li et al. 2018), with a mixed strategy: mostly focussing on extremely low-metallicity candidates, and partly randomly extending the sample up to $[\text{Fe}/\text{H}] = -2.0$ for bright stars (Aoki et al. 2022). The authors do not comment on possible selection effects towards or against carbon-rich stars in this process.

2.3 CEMP fractions in the *Pristine* survey

The *Pristine* survey uses narrow-band photometry combined with broad-band photometry to select metal-poor stars (Starkenburg et al. 2017). The *CaHK* filter employed by the *Pristine* survey is narrower than the v filter of the SkyMapper survey, and is expected to be less affected by molecular features in carbon-rich stars. However, *Pristine* also uses broad-band photometry, which can also be affected by carbon. The main *Pristine* survey, targeting the Galactic halo, has done extensive follow-up over the last years. We will discuss the CEMP fractions in various *Pristine* halo samples next.

2.3.1 The CEMP fraction in Aguado et al. (2019)

A sample of 1007 very metal-poor candidates followed up with medium-resolution was published in Aguado et al. (2019, hereafter AY19), analysed with the FERRE code⁴. Due to the relatively low signal-to-noise and the fact that many stars had relatively high temperatures, $[\text{C}/\text{Fe}]$ could only be reliably derived for a sample of 173 stars with $[\text{Fe}/\text{H}] < -2.0$. It was also not possible to derive good $\log g$ values and many stars had $\log g$ values close to the limit of the grid ($\log g = 1$ for giants). A bad $\log g$ is not expected to strongly affect the T_{eff} and $[\text{Fe}/\text{H}]$ values, but AY19 showed that there is a strong correlation between $\log g$ and $[\text{C}/\text{Fe}]$ in the FERRE analysis (also discussed in Arentsen et al. 2021). No corrections for this effect were applied in AY19, the uncertainties on $\log g$ were simply inflated accordingly. The authors concluded that the fraction of CEMP stars was consistent with the literature, with $41 \pm 4\%$ for VMP stars with $-3.0 < [\text{Fe}/\text{H}] < -2.0$ and $58 \pm 14\%$ for EMP stars with $[\text{Fe}/\text{H}] < -3.0$.

Here we apply empirical corrections to the $[\text{C}/\text{Fe}]$ values from AY19, based on the mean behaviour between $\log g$ and $[\text{C}/\text{Fe}]$ found in the FERRE analyses of AY19 and Arentsen et al. (2021), and quantified in Arentsen et al. (2021) as $\Delta[\text{C}/\text{Fe}] = -0.37\Delta \log g$. We determine the difference between the FERRE $\log g$ values and $\log g$ values adopted from Yonsei-Yale isochrones (Demarque et al. 2004) with an age of 12 Gyr in a grid from $-3.5 < [\text{Fe}/\text{H}] < -2.0$ in steps of 0.1 dex, and use this to estimate corrections to $[\text{C}/\text{Fe}]$. The

³ <http://www.lamost.org/public/?locale=en>

⁴ FERRE (Allende Prieto et al. 2006) is available from <http://github.com/callendeprieto/ferre>

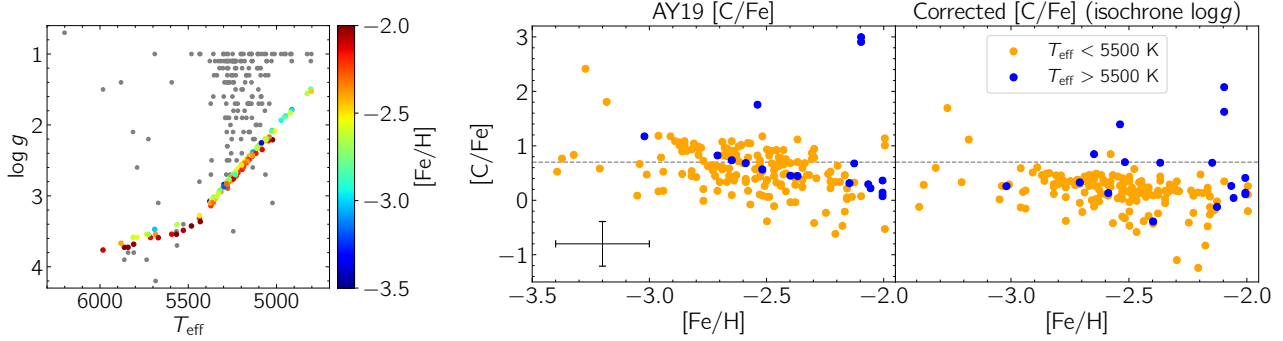


Figure 2. Determination of the $[C/Fe]$ correction for the sample of VMP stars from AY19 with reliable $[C/Fe]$. Left-hand panel: T_{eff} – $\log g$ diagram, with the FERRE $\log g$'s in grey and the isochrone $\log g$'s coloured by $[Fe/H]$ from FERRE. Right-hand panels: $[Fe/H]$ versus $[C/Fe]_{\text{AY19}}$ (left) or $[C/Fe]_{\text{iso}}$ (right), for cool stars with $T_{\text{eff}} < 5500$ K in orange and hotter stars in blue. The dashed line is placed at $[C/Fe] = +0.7$. The median uncertainties for $[Fe/H]$ and $[C/Fe]$ are shown on the bottom left of the AY19 $[C/Fe]$ panel.

results are shown in Figure 2, where the left-hand panel shows a Kiel diagram with the old (grey) and new (coloured) $\log g$ values. Most stars in the sample have $\log g_{\text{iso}} > 2.0$, therefore the $[C/Fe]$ should not yet be affected significantly by evolutionary effects along the RGB. The right-hand panels show the difference between the $[C/Fe]$ from AY19 and those corrected using the isochrone $\log g$ values. The total number of CEMP stars is reduced from 64 to 13 – these are the stars above the $[C/Fe] = +0.7$ lines in the right-hand panels. Additionally, the dispersion in $[C/Fe]$ reduces as well.

How does this $[C/Fe]$ correction affect the CEMP fraction in the AY19 sample? It varies with temperature and metallicity, as visible in the right-hand panels of Figure 2. For warm VMP stars with $T_{\text{eff}} > 5500$ K the CEMP fraction is $7/17 = 41.2\%$, which is comparable to what was reported in AY19. There is only one EMP star in this temperature range, and it is not carbon-rich. For cooler EMP stars with $5000 \text{ K} < T_{\text{eff}} < 5500 \text{ K}$ the fraction is $3/8 = 37.5\%$, consistent with AY19. For $[Fe/H] < -2.0$ in this temperature range, however, there is a strikingly low fraction of CEMP stars: only $3/135 = 2.2\%$. In fact none of these three has $[C/Fe] > +1.0$. This is in severe disagreement with previously derived CEMP fractions.

2.3.2 The CEMP fraction in other Pristine samples

In the *Pristine*-selected sample followed up with FORS2 medium-resolution spectroscopy by Caffau et al. (2020), the authors noted a lower CEMP fraction compared to AY19, with $3/28 = 11\%$ for $-3.0 < [Fe/H] < -2.0$ and $4/13 = 31\%$ for $[Fe/H] < -3.0$. If one only considers the stars in their sample with $T_{\text{eff}} < 5500$ K, actually none out of the 63 stars with $[Fe/H] < -2.0$ are considered CEMP, whereas for hotter stars the fraction is 32% ($8/25$).

Similar effects with temperature are seen in the high-resolution *Pristine* ESPaDOnS sample, by Lucchesi et al. (2022). The fraction of CEMP stars appears to be consistent with that of P14 for dwarfs/unevolved giants. For cooler giants, however, they find a CEMP fraction of only 11% , with none of the CEMP giants having $[C/Fe] > +1.0$.

In the *Pristine* Inner Galaxy Survey (PIGS, Arentsen et al. 2021), which contains only giant stars, the fractions of CEMP stars are found to be 5.7% for $[Fe/H] < -2.0$ and 16.4% for $[Fe/H] < -2.5$, both much lower than in P14. For $[Fe/H] < -3.0$, the CEMP fraction is consistent with P14. The authors interpret the discrepancy to be a combination of selection effects and a real difference in CEMP stars

between the inner Galaxy and the rest of the halo (see the discussion in Arentsen et al. 2021).

The general trend appears to be that the CEMP fractions in *Pristine* are largely consistent with previous estimates for extremely metal-poor stars and for warmer stars (e.g. $T_{\text{eff}} > 5500$ K), but not for cooler giants with $[Fe/H] > -3.0$. This is likely related to photometric selection effects, as for example in the SkyMapper survey (Da Costa et al. 2019), which will be discussed in a forthcoming paper.

2.4 Relative CEMP-no/s fractions

Above, we mainly discussed the fraction of CEMP stars with respect to carbon-normal stars. In several cases, separate fractions for CEMP-s and CEMP-no stars were reported as well. Since these CEMP types have very different progenitors, their relative fraction teaches us about the importance of the different physical processes with metallicity. Here we will compare a number of CEMP samples and the relative frequency of CEMP-no vs. CEMP-s stars.

A compilation of more than 300 CEMP stars ($[C/Fe] > +0.7$) which have high-resolution spectroscopy was published by Yoon et al. (2016). This sample does not contain carbon-normal stars and can therefore not be used to estimate the CEMP fraction, but it is an interesting sample to investigate the relative fraction of CEMP-s and CEMP-no stars. Given the inhomogeneity of the literature, it is not possible to say whether or not the sample is unbiased with respect to the different types of CEMP stars. Different selection biases may have canceled each other out, but it is not certain. For practical purposes, for now we assume that there is no (significant) bias towards a certain type of CEMP star at a given metallicity. There could conceivably be an overall bias towards more metal-poor stars in the sample, given previous follow-up strategies.

We determine the fraction of CEMP-no stars among all the CEMP stars in the Yoon et al. (2016) compilation, and also the fraction of Group II+III stars (these have been selected using A(C) instead of using $[Ba/Fe]$), which are expected to be similar (Yoon et al. 2016). The results for cumulative and differential fractions as a function of metallicity are shown in the top and bottom panels of Figure 3, respectively. Indeed they are similar for CEMP-no and Group II+III. The cumulative fraction is sensitive to the underlying metallicity distribution – the fractions for $[Fe/H] > -3.0$ are strongly affected by what happens at lower metallicities. This is especially true if a sample has relatively many extremely metal-poor stars compared to

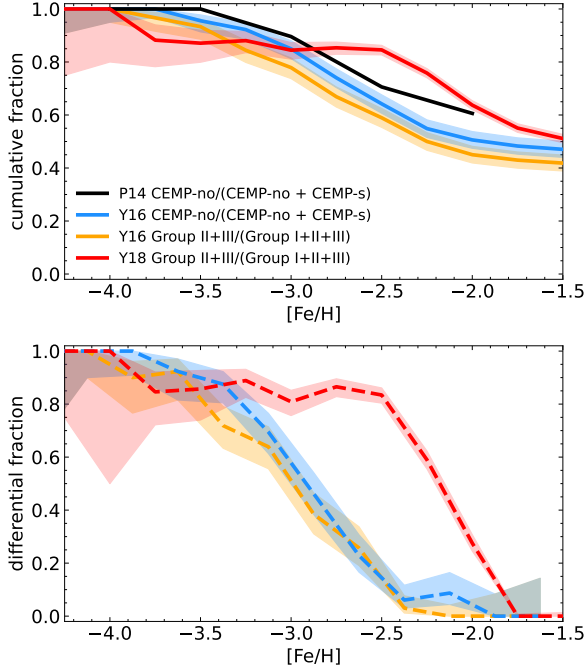


Figure 3. Fraction of CEMP-no (blue) or CEMP Group II+III (orange) stars among all classified CEMP stars in the Yoon et al. (2016) sample. The CEMP-no fraction from P14 is shown in black, the Group II+III fraction from Yoon et al. (2018) in red. The top and bottom panel show the cumulative fraction (for all stars below a certain $[\text{Fe}/\text{H}]$) and the differential fraction (for stars in a small range of $[\text{Fe}/\text{H}]$), respectively.

very metal-poor stars, which is often the case for high-resolution spectroscopic samples. The differential fractions are more relevant, they describe the relative importance of each type of CEMP star for a given metallicity bin. They clearly show that the CEMP-s/Group I stars dominate for $[\text{Fe}/\text{H}] > -3.0$ and the CEMP-no/Group II+III stars for $[\text{Fe}/\text{H}] < -3.0$.

The cumulative fractions of the high-resolution P14 compilation are also shown in black in the top panel of Figure 3. It follows the shape of the cumulative distribution in Yoon et al. (2016) – comparing the black and blue curves. This is not surprising, given that they are both based on similar literature samples. The P14 curve lies slightly higher, meaning larger fractions of CEMP-no stars, which may also be unsurprising given that they mainly set out to determine the CEMP-no fraction and therefore may have included fewer CEMP-s stars in the compilation.

Finally, the cumulative and differential fractions of Group II+III stars in the low-resolution Yoon et al. (2018) AEGIS sample are shown in red. They have a very different behaviour compared to the high-resolution samples – comparing to the orange curves for Yoon et al. (2016) Group II+III stars. AEGIS has both a higher cumulative and a higher differential fraction of Group II+III stars for $[\text{Fe}/\text{H}] > -3.0$, while it is slightly lower for extremely metal-poor stars. The difference is particularly striking for the differential fraction, which is the fairer comparison because it is not sensitive to the underlying metallicity distribution of the sample. The reasons for the difference in CEMP-no fraction between the samples is unclear. It could be related to selection effects in one or both samples – for example, AEGIS is a follow-up survey based on SkyMapper photometry, which could possibly have introduced a bias against the more carbon-rich Group I stars. The fraction could also be affected by the precision of derived $[\text{C}/\text{Fe}]$ and $[\text{Fe}/\text{H}]$ estimates from low-

resolution spectroscopy. This makes the division into the different CEMP groups using $A(\text{C})$ less precise. Having larger uncertainties also means that more stars may scatter above the $[\text{C}/\text{Fe}] > +0.7$ limit, into the region of Group II+III CEMP stars. This will be a topic of discussion in Section 3 as well.

2.5 Discussion on selection effects and biases

The goal of this section on the literature is to show how different various samples used for the determination of CEMP fractions are, how they may be plagued by different systematic issues, and how it can be difficult to compare them with each other. Although the general trend of an increasing CEMP fraction with decreasing metallicity is clear, there still exist discrepancies between the actual derived fractions that we do not yet understand.

The difficulty with high-resolution (and small) samples is that they are often selected for the most metal-poor stars (e.g. HK, HES), and they are not complete at higher metallicities ($[\text{Fe}/\text{H}] > -3.0$). Additionally, there are other human selection factors involved in the building of those samples as well, e.g., preference for or against carbon-rich stars, and these are hard to retrace for individual samples, let alone for literature compilations. The advantage of high-resolution spectroscopy is that the carbon abundances are (likely) more precisely determined.

The difficulty with low-resolution (often the larger, likely less biased) samples is that the stellar parameters and $[\text{C}/\text{Fe}]$ are more challenging to determine. Some biases were for example visible in the early $[\text{C}/\text{Fe}]$ estimates from Beers et al. (1998, 1999) mentioned above, or in the *Pristine* Aguado et al. (2019) analysis, discussed above as well. More on this topic will be discussed in Section 3. Low-resolution samples also have larger uncertainties associated with their $[\text{Fe}/\text{H}]$ and $[\text{C}/\text{Fe}]$ determinations, leading to more stars randomly scattering into the CEMP regime.

Finally, the difficulty with photometrically selected VMP samples (e.g. SkyMapper, *Pristine*) are the biases coming from colour selections. The photometry in different bands can be affected by large molecular carbon features, especially for the cooler carbon-rich objects.

All CEMP fractions discussed in this section are for samples of halo stars (except for PIGS). However, not all halo samples are the same. For example, they have different metallicity distributions, which strongly affects the derivation of *cumulative* CEMP fractions. If samples are large enough, *differential* fractions should be determined instead, making comparisons between samples more straightforward and less dependent on the underlying MDF. Additionally, different samples of halo stars can probe very different regions of the halo, for example because they select a different magnitude range, or use different tracers such as turn-off stars or giants. There may be real differences between CEMP fractions and the relative number of CEMP-s/-no stars in different parts of the Galaxy (as suggested by e.g. Frebel et al. 2006; Carollo et al. 2014; Lee et al. 2017, 2019; Yoon et al. 2018; Arentsen et al. 2021), but part of the observed differences may also be due to systematics caused by the use of different tracers, differences in spectral analysis pipelines and/or different assumptions for the synthetic grids. This makes comparisons between different samples even more challenging.

There is a huge caveat in *all* CEMP fraction determinations that we have not yet discussed. The iron and carbon abundances that go into these fractions are usually determined using synthetic spectra calculated in one dimension and in local thermodynamic equilibrium (LTE), but for very metal-poor stars the 3D and/or non-LTE effects on $[\text{Fe}/\text{H}]$ and/or $[\text{C}/\text{Fe}]$ can be large (e.g. Asplund 2005; Gallagher et al.

2017; Amarsi et al. 2019). Norris & Yong (2019) applied 3D and non-LTE corrections (based on computations in the literature for a small number of stars) to the CEMP sample of Yoon et al. (2016) and find that the number of stars that can be classified as CEMP drops by 70% after the corrections. For the sample of extremely metal-poor stars in Yong et al. (2013), the CEMP-no fraction drops from 24% to 8%. The impact of 3D/non-LTE on the CEMP fractions is significant, and, if correct, completely changes the picture. Preferentially, one would have 3D/non-LTE calculations for each star, but these are extremely expensive and this will not be possible in the near future.

While this means that we may not (yet) know the *absolute* number of CEMP stars, the hope is that it is still possible to compare the CEMP fraction between different samples and/or Galactic environments. Since 3D/non-LTE corrections depend on the evolutionary stage of a star, ideally, samples with stars in similar stages would be used for such comparisons. This is another reason why we mostly focus on giants in this work.

3 SPECTRAL ANALYSIS COMPARISON OF LOW-RESOLUTION VMP SAMPLES

It is clear from the previous section that low-resolution spectroscopic samples play a key role in understanding populations of CEMP stars. In this section, we compare various samples and analyses of low-resolution ($R \sim 1000\text{--}2000$) spectroscopic VMP stars to test whether their carbon abundances are on the same scale, and hence whether their CEMP fractions can be compared. We focus on giants in the metallicity range of $-3.0 < [\text{Fe}/\text{H}] < -2.0$, where both CEMP-no and CEMP-s stars are expected to be important and where there is still unclarity regarding the CEMP fraction for the two classes.

3.1 Carbon trends in various literature samples

We first compile a number of low-resolution VMP samples from the literature and study their $[\text{C}/\text{Fe}]$ trends to see if there are systematic differences between them. The main sample comes from the SDSS, analysed with the SSPP as described in Lee et al. (2013). Second, we use the VMP LAMOST DR3 sample (Yuan et al. 2020), whose spectra are quite similar to those from SDSS, analysed with the n-SSPP (Beers et al. 2014, 2017). Furthermore, we include the low-resolution optical follow-up from RAVE (Placco et al. 2018) and the Best & Brightest (B&B) survey (Placco et al. 2019; Limberg et al. 2021, recently superseded by Shank et al. 2021), analysed with the n-SSPP. Then, we include two samples analysed with FERRE (Allende Prieto et al. 2014), from the *Pristine* halo survey (AY19, $[\text{C}/\text{Fe}]$ corrected as described in the previous section) and from the *Pristine* Inner Galaxy Survey (PIGS, Arentsen et al. 2021). Finally, we compare with the P14 and Li et al. (2022) high-resolution samples.

We focus on cool giants ($T_{\text{eff}} < 5700$ K, $\log g < 3.8$) for the reasons described in the introduction, and mainly because the sample of warm stars is biased towards stars with higher carbon abundances due to difficulty in measuring carbon in warmer stars. We further limit our analysis to $-3.0 < [\text{Fe}/\text{H}] < -2.0$ because this is the metallicity range where the CEMP fraction is less well-constrained and the various low-resolution samples have most of their stars. We use carbon abundances with P14 evolutionary corrections where available (for the RAVE, B&B, PIGS and P14 samples, and we computed them for the Li et al. 2022 sample as well), and if they are not available (for the SDSS, LAMOST and *Pristine* samples) we limit ourselves to giants with $\log g > 2.3$, for which evolutionary effects are not yet important.

In the top panel of Figure 4, we show the mean carbon abundance with metallicity for the various samples. We only include stars not strongly enhanced or depleted in carbon ($-0.5 < [\text{C}/\text{Fe}] < +1.0$), to get a sense of the general trends. Although the trend is similar in each sample (increasing $[\text{C}/\text{Fe}]$ with decreasing $[\text{Fe}/\text{H}]$), there are large offsets between them, especially for $[\text{Fe}/\text{H}]$ higher than -2.5 . The FERRE samples more or less follow the Placco et al. (2014) high-resolution $[\text{C}/\text{Fe}]$, whereas the SDSS and LAMOST samples have a higher average $[\text{C}/\text{Fe}]$ by $0.14\text{--}0.17$ dex, and the n-SSPP samples a higher average $[\text{C}/\text{Fe}]$ by $0.22\text{--}0.32$ dex. It is notable that samples analysed with similar methods have similar systematic differences compared to the Placco et al. (2014) high-resolution trend.

In the bottom panels of Figure 4, we show the distributions of the VMP stars in each sample, this time including the CEMP stars. We also include the high-resolution CEMP compilation from Yoon et al. (2016), making the same cool giant cuts and adopting the carbon abundances with P14 evolutionary corrections. In both the P14 and Yoon et al. (2016) samples, almost all CEMP stars have $[\text{C}/\text{Fe}] > +1.5$, whereas in most of the low-resolution samples the majority of the CEMP stars is actually between $+0.7 < [\text{C}/\text{Fe}] < +1.0$ (and almost none with $[\text{C}/\text{Fe}] > +1.5$). In most low-resolution giant samples, especially those analysed with a version of the SSPP, $[\text{C}/\text{Fe}] > +0.7$ does not appear to be a natural division of carbon-normal and CEMP stars.

The CEMP distributions of VMP giants in low- and high-resolution samples are very different. This could be a reflection of the high-resolution follow-up efforts over the years – the interest was mostly in extremely metal-poor stars and very carbon-rich stars, and they may have a relative lack of more metal-rich, less carbon-rich stars. The Li et al. (2022) high-resolution spectroscopic follow-up LAMOST sample also does not have many very carbon-rich stars. This sample was chosen “randomly” from the VMP candidates sample in LAMOST (Aoki et al. 2022). However, even randomly selected samples can have selection effects, e.g. due to stars needing to be observable at the high-resolution facility at a given time. Additionally, the VMP candidates sample itself could already have biases against carbon-rich stars due to the analysis of the low-resolution spectra.

With the exception of the PIGS sample (which is in the inner Galaxy), all samples are supposed to be “typical” halo samples and there is therefore no expectation that the differences in the $[\text{C}/\text{Fe}]$ trend or distribution of CEMP stars would have a physical origin. Sample selection effects and/or differences in spectral analysis systematics must play an important role, and they strongly affect the derived CEMP fraction. Next, we compare the analyses from two different low-resolution spectral analysis tools to assess whether some of the systematic differences we have seen here can be clarified.

3.2 The SSPP and FERRE

Some of the differences in $[\text{C}/\text{Fe}]$ between various analyses/samples may come from systematic differences in the main stellar parameters (T_{eff} , $\log g$, $[\text{Fe}/\text{H}]$), due to degeneracies of $[\text{C}/\text{Fe}]$ with all of them. The other two parameters kept the same, the strength of the CH G-band decreases with increasing T_{eff} , with decreasing $\log g$ or with decreasing $[\text{Fe}/\text{H}]$. But there may also be more fundamental differences in the determination of $[\text{C}/\text{Fe}]$, even if all other parameters agree. We test this in this section.

Two commonly used codes to analyse low-resolution spectra of

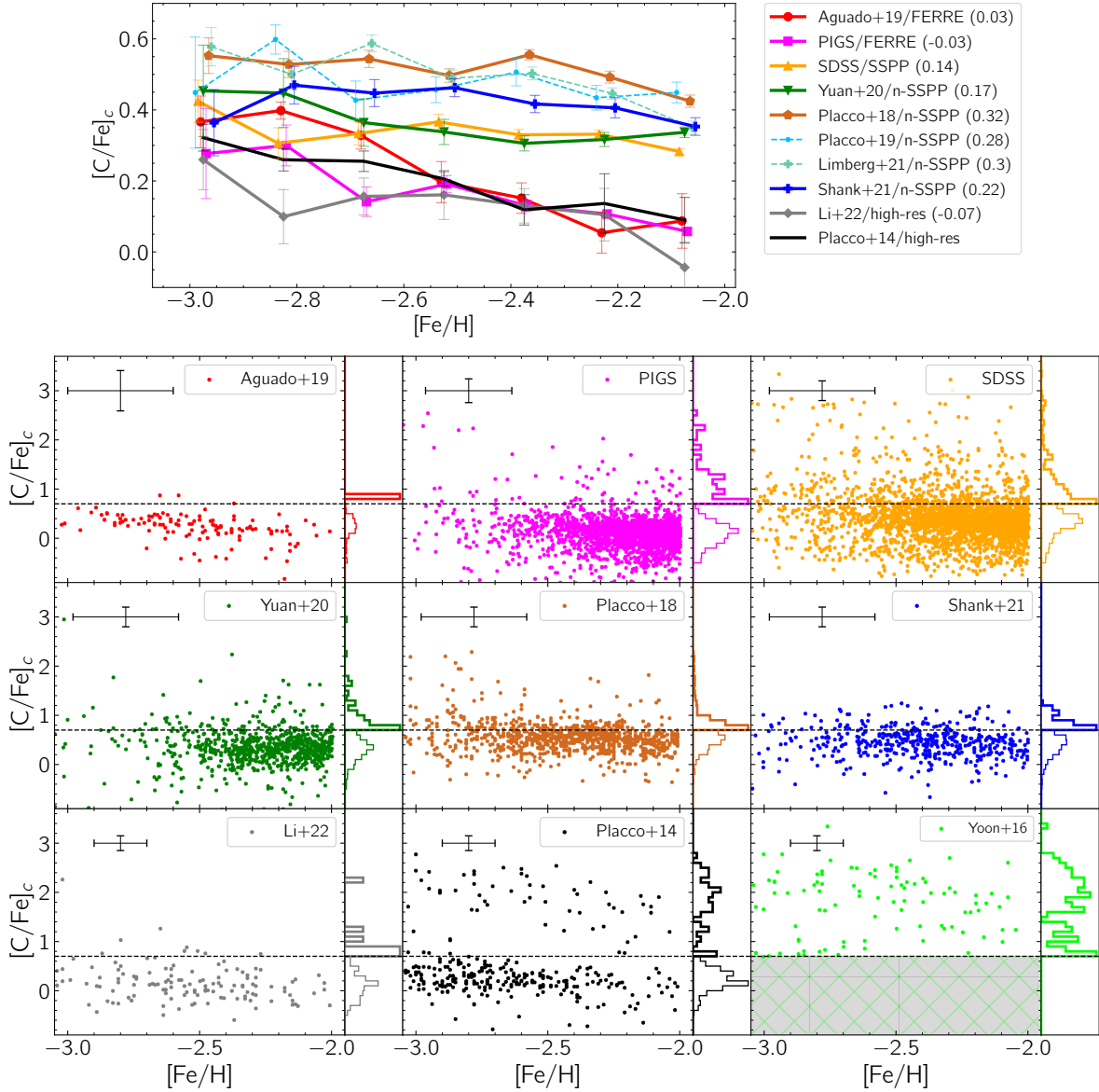


Figure 4. Top: the average $[C/Fe]_c$ with metallicity for relatively carbon-normal stars ($-0.5 < [C/Fe]_c < +1.0$) for various giant samples and methods (see text for details), where the error bars represent σ/\sqrt{N} . All included stars have been corrected for evolutionary effects, or have $\log g > 2.3$. Small offsets in $[Fe/H]$ have been applied for visibility of the error bars. The Placco et al. (2019) and Limberg et al. (2021) analyses were superseded by Shank et al. (2021), they are shown with dashed lines. In the legend, the average $[C/Fe]_c$ difference between the Placco et al. (2014) high-resolution trend and each sample is indicated in parenthesis. Bottom: distributions in $[Fe/H]$ and $[C/Fe]$ for the same samples, and an additional panel for the CEMP compilation by Yoon et al. (2016). The $[C/Fe]$ histograms are shown on the right-hand side of each panel, with the carbon-normal stars represented by thin lines and the CEMP stars by thick lines (separated at $[C/Fe] = +0.7$). They are normalised separately to highlight their distributions. Representative error bars are indicated in the top left of each panel – for the AY19 and PIGS samples this is the median of the provided individual uncertainties, for the (n-)SSPP samples this is 0.2 dex for both $[Fe/H]$ and $[C/Fe]$ (Lee et al. 2008a, 2013; Beers et al. 2014, 2017), and for the high-resolution samples they are 0.1 dex for $[Fe/H]$ and 0.15 dex for $[C/Fe]$.

VMP stars are the SSPP and FERRE. In FERRE⁵ (Allende Prieto et al. 2006), the four parameters T_{eff} , $\log g$, $[Fe/H]$ and $[C/Fe]$ are typically determined simultaneously. The application of FERRE to low-resolution spectra to derive these four parameters for VMP stars was first described in Aguado et al. (2017). Within the SSPP, the main stellar parameters T_{eff} , $\log g$ and $[Fe/H]$ are determined first (Lee et al. 2008a,b, 2013). They are derived by computing many different

spectroscopic and/or photometric estimates for each parameter and combining them to an adopted value. In a second step, T_{eff} and $\log g$ are fixed to the previously determined values, and only $[Fe/H]$ and $[C/Fe]$ can vary in a comparison with synthetic spectra in a limited wavelength range around the G-band (between 4290 – 4318 Å). The adopted $[C/Fe]$ comes from this second step.

Both methods use grids of synthetic spectra to derive stellar parameters and carbon abundances. Carbon enhancement strongly affects the structure of stellar atmospheres, resulting in differences in the synthesised stellar spectra. It is therefore important to use carbon-enhanced atmosphere models, which has been done for both the

⁵ FERRE is available from <http://github.com/callendeprieto/ferre>

SSPP and FERRE grids, although they have been computed using different models: for SSPP the MARCS models (Gustafsson et al. 2008) were used and for FERRE the Kurucz models (Mészáros et al. 2012). The spectra have been also been synthesised using different codes, namely TURBOSPECTRUM (Alvarez & Plez 1998; Plez 2012) for SSPP and ASSET (Koesterke et al. 2008) for FERRE. Different line lists were used as well, where most relevant here is what has been adopted for molecular carbon features – for SSPP those come from Masseron et al. (2014), while for FERRE the Kurucz⁶ line list was adopted. Additionally, different assumptions were made for the micro-turbulence, with a fixed value of $\xi_t = 2 \text{ km s}^{-1}$ for the FERRE grid (representative for giant stars) and adopting the relation $\xi_t [\text{km s}^{-1}] = -0.345 \cdot \log g + 2.225$ for the SSPP grid (derived from high-resolution spectra of SDSS/SEGUE stars used to calibrate the SSPP). Finally, both grids assume $[a/\text{Fe}] = +0.4$ for very metal-poor stars, but different assumptions were made for the nitrogen abundances: in the FERRE grid $[\text{N}/\text{Fe}] = 0.0$ and in the SSPP grid nitrogen follows carbon, meaning that $[\text{C}/\text{Fe}] = [\text{N}/\text{Fe}]$ (or $[\text{C}/\text{N}] = 0.0$). For stars with large carbon over-abundances, this makes a significant difference. Furthermore, these assumptions do not affect the analysis of all CEMP types in the same way, since the CNO abundances are different for CEMP-s and CEMP-no stars due to differences in the nucleosynthetic processes in AGB stars and the (supernovae of) the First Stars.

The different adopted synthetic grids may result in systematic differences in derived carbon abundances. We performed a preliminary analysis to test the magnitude of this effect, fitting spectra from the SSPP grid with FERRE and spectra from the n-SSPP grid with FERRE. Details are given in Appendix A. In summary, we find that for stars with $[\text{C}/\text{Fe}] < +1.5$ there can be systematics in $[\text{C}/\text{Fe}]$ of $\sim 0.1 - 0.2$ dex, depending on the T_{eff} and the adopted pipeline.

For n-SSPP analyses, additional empirical corrections based on a comparison with high-resolution spectroscopy are usually applied to each of the four parameters (Beers et al. 2014). These corrections have been determined for a mixture of stars of different temperatures, evolutionary phases and metallicities, and are only a function of the parameter itself (no cross-terms with other parameters). Conceivably, these corrections could be quite different for stars of different types. This should be tested in the future. For $[\text{C}/\text{Fe}]$, the parameter of most interest in this paper, the empirical correction is the following: $[\text{C}/\text{Fe}]_{\text{B14}} = [\text{C}/\text{Fe}] - (-0.068 \times [\text{C}/\text{Fe}] + 0.273)$. It is therefore of the order of -0.2 to -0.3 dex for carbon-normal stars ($-0.5 < [\text{C}/\text{Fe}] < +1.0$).

3.3 Direct comparisons of SSPP and FERRE analyses

The analysis of low-resolution spectra of cool, very carbon-rich stars is a particularly challenging task (see e.g. discussions in Beers et al. 1999; Rossi et al. 2005; Goswami et al. 2006; Yoon et al. 2020). It is beyond the scope of this paper to investigate in detail the differences for very carbon-rich stars. For example, it would be important to further analyse the underlying assumptions in the synthetic spectroscopy grids used (especially the adopted CNO abundances) and/or whether photometry is included or not in the parameter determination. Instead, we focus on carbon-normal stars and stars are not very carbon-enhanced ($[\text{C}/\text{Fe}] < +1.0$) in this section, where we directly compare results from the (n-)SSPP and FERRE.

3.3.1 Re-analysis of SDSS, LAMOST and RAVE follow-up with FERRE

Using the FERRE code, we re-analyse stars from three different halo samples previously analysed with the (n-)SSPP. We select random cool, carbon-normal ($[\text{C}/\text{Fe}] < +1.0$) VMP giants in the same $T_{\text{eff}} - \log g$ range as in Section 3.1 from the SDSS (700 stars, $R \sim 2000$, $3850 - 9200 \text{ \AA}$), analysed with the SSPP, and the LAMOST VMP sample of Yuan et al. (2020) (400 stars, $R \sim 1800$, $3700 - 9000 \text{ \AA}$), analysed with the n-SSPP. We apply a signal-to-noise (S/N) cut of $\text{S/N} > 20$. We additionally select all VMP giants from the optical RAVE follow-up from Placco et al. (2018) observed with KPNO/Mayall-RC (80 stars, $R \sim 1500$, $3500 - 6000 \text{ \AA}$) and ESO/NTT (160 stars, $R \sim 1200$, $3300 - 5100 \text{ \AA}$), analysed with the n-SSPP. The spectra in these samples typically have very high S/N, because they are the follow-up of bright stars. We do not apply P14 evolutionary carbon corrections to any of the sample $[\text{C}/\text{Fe}]$ values, because here we are only interested in the comparison between direct results from the spectroscopic analyses. For the RAVE samples, Placco et al. (2018) applied the Beers et al. (2014) empirical n-SSPP corrections to the n-SSPP output.

The synthetic spectral grid used in the FERRE analysis is an extension of the grid published in Aguado et al. (2017) to lower temperatures and higher metallicities, and has free parameters T_{eff} , $\log g$, $[\text{Fe}/\text{H}]$ and $[\text{C}/\text{Fe}]$ (first used in Arentsen et al. 2020, see details there). We use the cubic Bézier interpolation in the models, and search for the best fit using the Nelder-Mead algorithm. The synthetic spectra are smoothed to the respective observed spectral resolutions, and the observed and synthetic spectra are normalised using a running mean of 30 pixels. We limit the fitted wavelength range to $3700 - 5500 \text{ \AA}$, or the available part thereof.

The comparison between the parameters from our FERRE analysis and the published values from the (n-)SSPP analyses is shown in Figure 5 (some cross-comparisons can be found in Figure C1 in Appendix C), with the SDSS and Yuan et al. (2020)/LAMOST samples in the left-hand column in green and orange, respectively, and the two RAVE/Placco et al. (2018) samples in the middle column. In this work we will not investigate the origins of all the stellar parameter differences between various methods and samples in detail, but we will focus on a few key observations regarding $[\text{C}/\text{Fe}]$.

For the SDSS and RAVE/NTT samples, the agreement between the stellar parameters (T_{eff} , $\log g$, $[\text{Fe}/\text{H}]$) from FERRE and those from the original (n-)SSPP analyses is in general excellent (except for the lower temperatures for SDSS, with $T_{\text{eff}}(\text{orig}) < 5000 \text{ K}$ – this is likely a bias in the FERRE analysis, see Appendix B. The $[\text{C}/\text{Fe}]$ values for these two samples are, however, systematically offset compared to the FERRE analysis, despite the main stellar parameters typically being in good agreement. For the other two samples, from LAMOST and RAVE/Mayall, the agreement for the stellar parameters is less good between the original and the FERRE analysis – there are systematic offsets. There is also a difference in the $[\text{C}/\text{Fe}]$ values.

The mean $\Delta[\text{C}/\text{Fe}]$ (original – FERRE) for the SDSS, LAMOST, RAVE/Mayall and RAVE/NTT samples is $+0.19$, $+0.22$, $+0.18$ and $+0.39$, respectively. For the SDSS and LAMOST analyses the stars with $T_{\text{eff}}(\text{original}) < 5000 \text{ K}$ have been excluded in this comparison, because they show a clear T_{eff} systematic in the comparison with FERRE. The differences between the (n-)SSPP and FERRE carbon abundances are of similar magnitudes as the differences seen in the $[\text{C}/\text{Fe}]$ trends in Figure 4 between the (n-)SSPP samples and the high-resolution trend.

From Figure 5 it can be seen that the difference in $[\text{C}/\text{Fe}]$ seems to be larger for relatively carbon-rich ($[\text{C}/\text{Fe}]_{(\text{n-})\text{SSPP}} > +0.4$) stars,

⁶ <http://kurucz.harvard.edu/linelists.html>

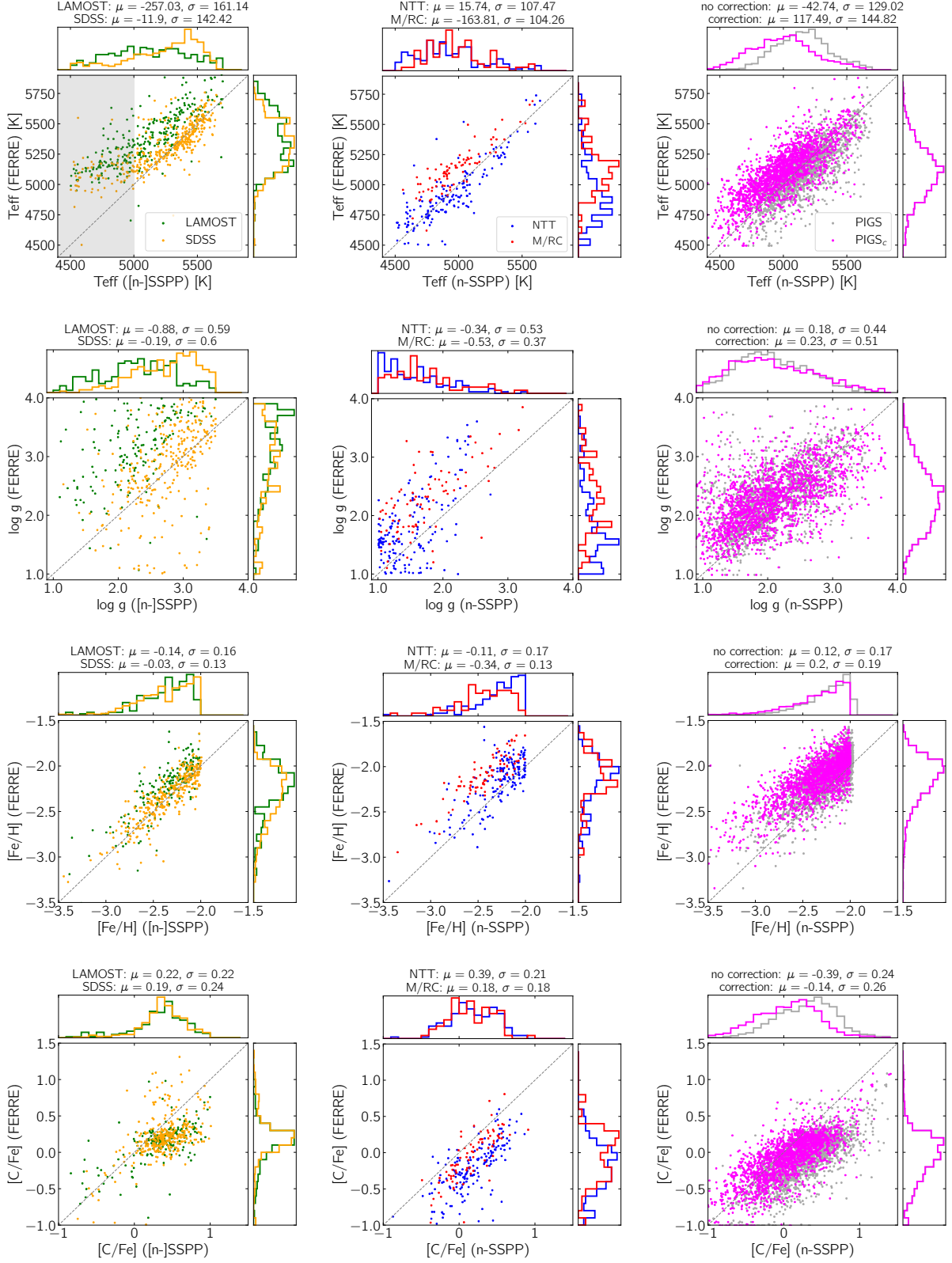


Figure 5. Comparison of (n)-SSPP versus FERRE parameters, for samples from SDSS and LAMOST (left-hand column, orange and green, respectively), the RAVE follow-up by Placco et al. (2018) for two different instruments (middle column) and PIGS (right-hand column, magenta and grey for n-SSPP results with or without Beers et al. (2014) corrections applied, respectively). The median and standard deviation of $\Delta\text{par} = \text{FERRE} - (\text{n-SSPP})$ are indicated in the title of each panel. For the SDSS/LAMOST panels, the stars with (n)-SSPP $T_{\text{eff}} < 5000$ K (the shaded region in the T_{eff} panel) have not been included in the $\log g$, $[\text{Fe}/\text{H}]$ and $[\text{C}/\text{Fe}]$ panels.

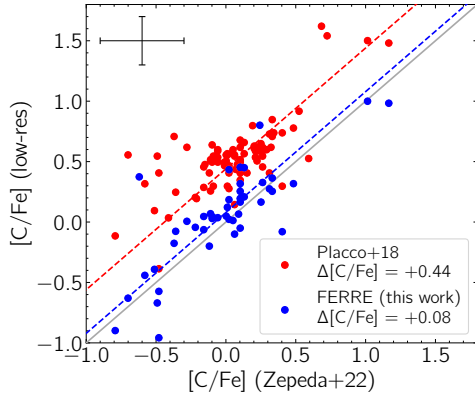


Figure 6. Comparison of high-resolution $[C/Fe]$ from Zepeda et al. (2022) and low-resolution $[C/Fe]$ from Placco et al. (2018) in red and FERRE (this work) in blue. Median differences between the high and low-resolution abundances have been indicated in the legend and are represented with coloured dashed lines.

especially for the SDSS and LAMOST samples. Limiting the comparison to these stars, $\Delta[C/Fe]$ (original – FERRE) further increases to +0.33 and +0.31 for SDSS and LAMOST, respectively.

Some of the $[C/Fe]$ differences between samples may be due to stellar parameter differences. To quantify the differences in $[C/Fe]$ that are *not* caused by the other stellar parameters, we make a comparison of stars with excellent agreement with the FERRE parameters only. For the best stars ($\Delta T_{\text{eff}} < 50$ K, $\Delta[Fe/H] < 0.05$ dex and $\Delta \log g < 0.5$ dex), we find that there is still a systematic difference in the $[C/Fe]$ values in the SDSS sample. For the 55 stars that remain, we find $\Delta[C/Fe](\text{original} - \text{FERRE}) = +0.22$. This goes up to +0.35 (based on 24 stars) for moderately carbon-rich stars ($[C/Fe]_{\text{SSPP}} > +0.4$). The other samples do not have enough stars with the strict comparison cuts. Increasing ΔT_{eff} to 100 K and $\Delta[Fe/H]$ to 0.1 dex, there are 18 stars in the NTT sample, for which $\Delta[C/Fe](\text{original} - \text{FERRE}) = +0.27$.

Finally, for the RAVE follow-up sample, we compare the low-resolution $[C/Fe]$ values directly with those from high-resolution spectroscopy from Zepeda et al. (2022), see Figure 6. Most stars are from the NTT sample. There is a similarly large offset between the Placco et al. (2018) and high-resolution carbon abundances as before, whereas the FERRE carbon abundances more closely resemble the high-resolution results.

3.3.2 Re-analysis of PIGS with n-SSPP

We perform a similar exercise as above with the *Pristine* Inner Galaxy Survey (PIGS) data, which have previously been analysed with FERRE (Arentsen et al. 2020) and which we now re-analyse with the n-SSPP. The PIGS data consist of two arms: one optical low-resolution arm ($R \sim 1300, 3700 - 5500$ Å) and one infrared medium-resolution arm ($R \sim 11000, 8400 - 8800$ Å). Both were used in the FERRE analysis, but here we use only the blue arm for the n-SSPP analysis, combined with 2MASS J and K photometry (Skrutskie et al. 2006). Since the n-SSPP uses photometry, the results could be affected by incorrect corrections for the high extinction in the bulge region. However, since the used photometry is in the infrared, we expect the effect to be minimal.

For each of the stellar parameters T_{eff} , $\log g$ and $[Fe/H]$, two versions are included in the n-SSPP output, namely A (adopted) and B (a bi-weight estimate). We use the adopted values, and use the dif-

ference between $[Fe/H]_A$ and $[Fe/H]_B$ as an extra quality cut. The carbon routine keeps T_{eff} and $\log g$ fixed to the adopted values and derives $[C/Fe]_{\text{car}}$ and $[Fe/H]_{\text{car}}$, which together provide $[C/H]$. The adopted carbon abundance is $[C/Fe]_A = [C/H] - [Fe/H]_A$. Finally, we apply the Beers et al. (2014) n-SSPP parameter corrections to the adopted parameters.

We only consider stars passing all FERRE quality criteria (see Arentsen et al. 2020), and we additionally cut stars with $|([Fe/H]_A - [Fe/H]_B)| > 0.2$ dex, uncertainty in J and K > 0.15 mag, number of T_{eff} estimates going into $T_{\text{eff},A} \leq 9$ or number of $[Fe/H]$ estimates going into $[Fe/H]_A \leq 3$. These cuts are relatively strict, but leave us with a cleaner sample for the comparison. Limiting the sample to the same stellar parameter space as in the previous section, we are left with 1600 cool VMP giants.

The comparison between the FERRE and n-SSPP analyses is shown in magenta in the right-hand column of Figure 5. We also include the parameters before applying the Beers et al. (2014) correction in grey. We make a few observations. First, for $[C/Fe]$, the corrections appear to improve the agreement between FERRE and the n-SSPP, but they make the agreement slightly worse for $[Fe/H]$ and significantly worse for T_{eff} . This might be a hint that the n-SSPP corrections are not entirely applicable for giant VMP stars. It could also mean that the FERRE temperatures are off. Second, after the corrections, there are systematic differences in all parameters, and for $[C/Fe]$ the difference is +0.13. The $[C/Fe]$ discrepancy becomes more severe for more carbon-rich stars with $[C/Fe]_{\text{SSPP}} > 0.0$ and +0.4, with $\Delta[C/Fe]$ going up to +0.23 and +0.36, respectively. Restricting the sample to stars which are in excellent agreement ($\Delta T_{\text{eff}} < 50$ K, $\Delta[Fe/H] < 0.05$ dex and $\Delta \log g < 0.5$ dex), we find $[C/Fe]$ to be relatively consistent ($\Delta[C/Fe](\text{n-SSPP} - \text{FERRE}) = -0.03$, based on 60 stars), and $\Delta[C/Fe] = +0.04$ for stars with $[C/Fe]_{\text{SSPP}} > 0.0$, based on 33 stars. The discrepancy in n-SSPP vs. FERRE $[C/Fe]$ for PIGS appears to be largely driven by the differences in the other stellar parameters, mostly the difference in metallicity.

Since the average $[C/Fe]$ is higher in the n-SSPP than in the original FERRE analysis, especially for stars with n-SSPP $[C/Fe] > +0.4$, the n-SSPP CEMP fraction in PIGS would increase compared to the published fraction in Arentsen et al. (2021). However, most of those new CEMP stars would have $+0.7 < [C/Fe] < +1.0$ and would not be clearly separate from the distribution of carbon-normal stars, whereas the CEMP stars identified in the original FERRE analysis are.

3.3.3 The $[C/Fe]$ distribution of carbon-normal stars

It can be seen in Figure 5 that there are almost no stars in the different FERRE analyses with $[C/Fe]_{\text{FERRE}} > +0.3/+0.4$ – there appears to be a limit in $[C/Fe]$ for carbon-normal stars. In the sample of VMP stars with high-resolution spectroscopy by P14 there is also an upper bound to $[C/Fe]$ for carbon-normal stars, which is around +0.4 for stars with $-2.6 < [Fe/H] < -2.0$ and around +0.7 for stars down to $[Fe/H] = -3.0$ (see Figure 4). In the SSPP-type analyses, the distribution is smoother and there does not appear to be a clear separation between carbon-normal and carbon-rich stars. This smoothness can also be seen in some of the (n-)SSPP samples shown in the bottom panels of Figure 4.

The smoother distributions for the (n-)SSPP samples could point to larger uncertainties in the abundances from those analyses compared to the FERRE analyses. Although the pipelines use the same spectra to derive $[C/Fe]$, the (n-)SSPP only uses a very small wavelength range centred on the G-band, whereas FERRE uses a much larger wavelength range. An alternative possibility is that there could be a limitation in the FERRE code and/or synthetic grid leading to a

spurious upper $[C/Fe]$ limit for carbon-normal stars. However, in the synthetic grid cross-analysis in Appendix B we find no obvious discontinuities in the derivation of $[C/Fe]$ from FERRE for stars with $[C/Fe] < +1.5$.

3.4 Summary: $[C/Fe]$ in low-resolution giant samples

We compared the trend of $[C/Fe]$ as a function of $[Fe/H]$ for carbon-normal giant stars in various low-resolution spectroscopic VMP samples, and found that there are systematic differences in $[C/Fe]$ between different samples analysed with different methods. Additionally, none of the samples have a CEMP star distribution similar to the CEMP stars in the high-resolution spectroscopic compilation of P14 or Yoon et al. (2016) – they all have a relatively low number of CEMP stars with $[C/Fe] > +1.5$.

We re-analysed low-resolution spectra of various samples of VMP giants to be able to directly compare the parameters from different methods, namely (versions of) the SSPP and FERRE. We focussed on stars with low/intermediate carbon abundances ($[C/Fe] < +1.0$). There are systematic differences in the determination of $[C/Fe]$ between FERRE and (versions of) the SSPP, of the order of 0.1–0.4 dex (with the SSPP analyses finding systematically higher $[C/Fe]$). The $[C/Fe]$ systematics become worse for stars with higher $[C/Fe]_{SSPP}$ (starting at $[C/Fe]_{SSPP} > 0.0$, and worse for $> +0.4$).

These differences are partly the result of systematic differences in the stellar parameters, because $[C/Fe]$ is very sensitive to T_{eff} , $\log g$ and $[Fe/H]$, but also partly *independent* of degeneracies with the other stellar parameters. This is possibly the result of other differences in the analysis pipelines, such as the fitting methods and/or the synthetic spectra, as discussed briefly in Appendix A.

The quoted uncertainties on $[C/Fe]$ estimates from low-resolution spectroscopy are typically of the order of $\sim 0.2 - 0.3$ dex (e.g. Lee et al. 2013; Arentsen et al. 2021). The offsets we have determined are smaller than or similar to these uncertainties. However, they cannot be ignored – a systematically larger $[C/Fe]$ will lead to larger fractions of CEMP stars. Many of the CEMP stars in low-resolution samples have $+0.7 < [C/Fe] < +1.0$ (see the bottom panels of Figure 4), hence the effect of a small offset can be large, especially when the uncertainties on $[Fe/H]$ and $[C/Fe]$ are large as well. The CEMP fraction for low-resolution samples is more sensitive to the exact CEMP definition, $[C/Fe] > +0.7$ or the more conservative $[C/Fe] > +1.0$, than the CEMP fraction for high-resolution samples.

4 CONCLUSIONS

The frequencies of (different sub-classes of) CEMP stars in astrophysical different environments probe the properties of the First Stars, the early chemical evolution, and the number of interacting binary stars in those environments. In this work, we investigate whether directly comparing the CEMP fractions for various samples of giant stars from different surveys is a valid approach. To do so, we compile and compare the overall behaviours of different published CEMP fractions and distributions. Further, we make a direct comparison of carbon abundances from two different analysis methods, FERRE versus versions of the SSPP, for several low-resolution spectroscopic samples. Our results can be summarised as follows:

- There are various challenges when determining CEMP fractions, affecting each sample differently, such as selection effects and/or assumptions, uncertainties and biases in the spectral analysis. In particular, it is important to compare samples of stars of similar evolutionary stages to minimise such biases.

- The published CEMP frequencies for different spectroscopic samples of halo giant stars do not always agree with one another, as summarised in Figure 1 and Table 1, although all frequencies are generally increasing with decreasing metallicity. The relative frequencies of CEMP-s and CEMP-no (or Group I and Group II+III, respectively) stars between low- and high-resolution spectroscopic samples also do not agree with each other (Figure 3 and the bottom panels of Figure 4).

- We suspect that high-resolution spectroscopic compilations of very metal-poor stars might be biased towards (very) carbon-rich objects at the “high” metallicity end ($[Fe/H] > -3.0$ and especially $[Fe/H] > -2.5$) due to their follow-up strategies. This leads to an over-estimate of the CEMP fraction in this metallicity range.

- We found that there are systematic differences in $[Fe/H]$ versus $[C/Fe]$ trends among various very metal-poor halo giant samples. We tested the role of the adopted pipeline for low-resolution spectroscopic samples by re-analysing stars from various surveys with the SSPP or FERRE, to compare the resulting stellar parameters and $[C/Fe]$ for carbon-normal stars ($[C/Fe] < +1.0$). The $[C/Fe]$ from the SSPP is typically $\sim 0.15 - 0.2$ dex higher than the $[C/Fe]$ from FERRE, even after taking into account degeneracies between $[C/Fe]$ and other stellar parameters. Some of this may be due to the use of different synthetic grids in the two pipelines.

- Systematic differences in $[C/Fe]$ can severely affect derived CEMP fractions, especially in low-resolution spectroscopic samples, which appear to have most of their CEMP stars in the range $+0.7 < [C/Fe] < +1.0$ and have large $[Fe/H]$ and $[C/Fe]$ uncertainties. This complicates the comparisons of CEMP fractions between different samples.

- Finally, we find that the frequency of CEMP stars in the low-resolution spectroscopic follow-up of the *Pristine* survey is lower than previously reported in Aguado et al. (2019) due to a systematic effect in $\log g$, with a complete lack of CEMP stars with $[C/Fe] > +1.0$ for $-3.0 < [Fe/H] < -2.0$. The low CEMP fraction and lack of very carbon-rich stars may be the result of photometric selection effects.

Due to the inconsistent results in CEMP fractions from different methods and surveys, we provide the following recommendations for publishing CEMP fractions in future work:

- It is more insightful to derive differential fractions (in bins of $[Fe/H]$) instead of cumulative fractions (all stars below a given $[Fe/H]$), because cumulative fractions depend on the underlying metallicity distribution function, which is not the same between different samples.

- Apart from employing the typical CEMP definition of $[C/Fe] > +0.7$, it would be useful to also derive the fraction of stars with very high carbon abundances (e.g. $[C/Fe] > +1.5$), to probe differences in the carbon distributions between samples. For example, in this work we highlighted that most low-resolution spectroscopic samples lack very carbon-rich stars compared to high-resolution samples. Additionally, these very carbon-rich stars are less likely to become non-CEMP after e.g. 3D/NLTE corrections.

We have already learned a lot from previous work on CEMP stars. However, due to the systematics between different large low-resolution spectroscopy samples of VMP and CEMP stars in the literature, it is still difficult to compare them directly and draw conclusions about differences or similarities between the properties of different Galactic environments. However, there are several ways to make progress in this area in the near future. These include:

- performing more homogeneous analyses of different samples to allow for their direct comparisons (although there will always be

some differences in the data, e.g. wavelength coverage and/or spectral resolution). This should likely also include a more sophisticated treatment of the uncertainties on [Fe/H] and [C/Fe], e.g. using Bayesian methods to derive statistical CEMP frequencies.

- deriving good estimates of selection biases in large previous, ongoing and upcoming spectroscopic surveys. This requires the selection function of surveys to be well-characterised, for which it is necessary to know how carbon-rich stars behave in various photometric bands. It would be useful to have access to carbon-enhanced stellar isochrones, for example.

- using samples without strong selection effects due to limited follow-up, such as purely photometric surveys and/or the Gaia DR3 spectrophotometry (although these samples could still be biased in other ways).

- making more direct comparisons of different pipelines and synthetic spectra to understand systematic differences, and improve the synthetic spectra and the assumptions that go into them. This likely should also include taking into account 3D/non-LTE effects on [Fe/H] and [C/Fe] in the future, although this is presently computationally very expensive.

Thanks to ongoing and upcoming large spectroscopic surveys such as WEAVE (Dalton et al. 2018), 4MOST (de Jong et al. 2019) and DESI (DESI Collaboration et al. 2016), there will soon be much larger samples of very metal-poor stars than before, and with higher spectral resolution. These surveys will be a treasure trove for Galactic Archaeology with CEMP stars.

ACKNOWLEDGEMENTS

We thank Kim Venn, Lyudmila Mashonkina, Zhen Yuan, Martin Montelius, and other members of the Pristine collaboration for valuable discussions or insightful comments on a draft of this work. We thank Tadafumi Matsuno for sharing the Li et al. (2022) data before their final publication.

AA and NFM gratefully acknowledge funding from the European Research Council (ERC) under the European Unions Horizon 2020 research and innovation programme (grant agreement No. 834148). The work of VMP is supported by NOIRLab, which is managed by the Association of Universities for Research in Astronomy (AURA) under a cooperative agreement with the National Science Foundation. YSL acknowledges support from the National Research Foundation (NRF) of Korea grant funded by the Ministry of Science and ICT (NRF-2021R1A2C1008679). DSA acknowledges support from ERC Starting Grant NEFERTITI H2020/808240. NFM gratefully acknowledge support from the French National Research Agency (ANR) funded project “Pristine” (ANR-18-CE31-0017). ES acknowledges funding through VIDI grant “Pushing Galactic Archaeology to its limits” (with project number VI.Vidi.193.093) which is funded by the Dutch Research Council (NWO).

AA, DSA, NFM and ES thank the International Space Science Institute, Bern, Switzerland for providing financial support and meeting facilities to the “Pristine” and “The early Milky Way” international teams.

Based on data obtained at Siding Spring Observatory (via programs S/2017B/01, A/2018A/01, OPTICON 2018B/029 and OPTICON 2019A/045, PI: A. Arentsen and A/2020A/11, PI: D. B. Zucker). We thank the Australian Astronomical Observatory, which have made the PIGS observations possible. We acknowledge the traditional owners of the land on which the AAT stands, the Gamilaraay people, and pay our respects to elders past and present.

Horizon 2020: This project has received funding from the European Union’s Horizon 2020 research and innovation programme under grant agreement No 730890. This material reflects only the authors views and the Commission is not liable for any use that may be made of the information contained therein.

Based on observations at Kitt Peak National Observatory at NSF’s NOIRLab (NOIRLab Prop. ID 14A-0323, 14B-0231, 15A-0071, 15B-0071, 17A-0295; PI: V. Placco), which is managed by the Association of Universities for Research in Astronomy (AURA) under a cooperative agreement with the National Science Foundation. The authors are honored to be permitted to conduct astronomical research on Iolkam Du’ag (Kitt Peak), a mountain with particular significance to the Tohono O’odham.

Based on observations collected at the European Organisation for Astronomical Research in the southern hemisphere under ESO programme(s) 095.D-0202(A), 096.D-0018(A), 097.D0196(A), 098.D-0434(A), and 099.D-0428(A).

Funding for the SDSS and SDSS-II has been provided by the Alfred P. Sloan Foundation, the Participating Institutions, the National Science Foundation, the U.S. Department of Energy, the National Aeronautics and Space Administration, the Japanese Monbukagakusho, the Max Planck Society, and the Higher Education Funding Council for England. The SDSS Web Site is <http://www.sdss.org/>. The SDSS is managed by the Astrophysical Research Consortium for the Participating Institutions. The Participating Institutions are the American Museum of Natural History, Astrophysical Institute Potsdam, University of Basel, University of Cambridge, Case Western Reserve University, University of Chicago, Drexel University, Fermilab, the Institute for Advanced Study, the Japan Participation Group, Johns Hopkins University, the Joint Institute for Nuclear Astrophysics, the Kavli Institute for Particle Astrophysics and Cosmology, the Korean Scientist Group, the Chinese Academy of Sciences (LAMOST), Los Alamos National Laboratory, the Max-Planck-Institute for Astronomy (MPIA), the Max-Planck-Institute for Astrophysics (MPA), New Mexico State University, Ohio State University, University of Pittsburgh, University of Portsmouth, Princeton University, the United States Naval Observatory, and the University of Washington.

Guoshoujing Telescope (the Large Sky Area Multi-Object Fiber Spectroscopic Telescope LAMOST) is a National Major Scientific Project built by the Chinese Academy of Sciences. Funding for the project has been provided by the National Development and Reform Commission. LAMOST is operated and managed by the National Astronomical Observatories, Chinese Academy of Sciences.

This work has made use of data from the European Space Agency (ESA) mission *Gaia* (<https://www.cosmos.esa.int/gaia>), processed by the *Gaia* Data Processing and Analysis Consortium (DPAC, <https://www.cosmos.esa.int/web/gaia/dpac/consortium>). Funding for the DPAC has been provided by national institutions, in particular the institutions participating in the *Gaia* Multilateral Agreement.

This research has made use of the MATPLOTLIB (Hunter 2007), NUMPY (Harris et al. 2020), PANDAS (McKinney 2010), DUSTMAPS (Green 2018) and ASTROPY (Astropy Collaboration et al. 2013; Price-Whelan et al. 2018) Python packages and of TOPCAT (Taylor 2005). We also used the spectroscopic analysis pipelines n-SSPP (Beers et al. 2014) and FERRE (Allende Prieto et al. 2014).

DATA AVAILABILITY

The SSPP analysis of the SDSS spectra with [C/Fe] values and the Placco et al. (2018) spectra will be shared on reasonable request to

Y. S. Lee and V. M. Placco, respectively. All other data underlying this article that is not public will be shared on reasonable request to A. Arentsen.

REFERENCES

- Abate C., Pols O. R., Karakas A. I., Izzard R. G., 2015, *A&A*, **576**, A118
- Aguado D. S., González Hernández J. I., Allende Prieto C., Rebolo R., 2017, *A&A*, **605**, A40
- Aguado D. S., et al., 2019, *MNRAS*, **490**, 2241
- Aguado D. S., et al., 2021, *MNRAS*, **500**, 889
- Allende Prieto C., Beers T. C., Wilhelm R., Newberg H. J., Rockosi C. M., Yanny B., Lee Y. S., 2006, *ApJ*, **636**, 804
- Allende Prieto C., et al., 2014, *A&A*, **568**, A7
- Alvarez R., Plez B., 1998, *A&A*, **330**, 1109
- Amarsi A. M., Nissen P. E., Asplund M., Lind K., Barklem P. S., 2019, *A&A*, **622**, L4
- Aoki W., Beers T. C., Christlieb N., Norris J. E., Ryan S. G., Tsangarides S., 2007, *ApJ*, **655**, 492
- Aoki W., et al., 2013, *AJ*, **145**, 13
- Aoki W., et al., 2022, arXiv e-prints, p. arXiv:2203.11505
- Arentsen A., Starkenburg E., Shetrone M. D., Venn K. A., Depagne É., McConnachie A. W., 2019, *A&A*, **621**, A108
- Arentsen A., et al., 2020, *MNRAS*, **496**, 4964
- Arentsen A., et al., 2021, *MNRAS*, **500**, 4348
- Asplund M., 2005, *ARA&A*, **43**, 481
- Astropy Collaboration et al., 2013, *A&A*, **558**, A33
- Barklem P. S., et al., 2005, *A&A*, **439**, 129
- Beers T. C., Christlieb N., 2005, *ARA&A*, **43**, 531
- Beers T. C., Preston G. W., Shectman S. A., 1992, *AJ*, **103**, 1987
- Beers T. C., Rossi S., Norris J. E., Ryan S. G., Molaro P., Rebolo R., 1998, *Space Sci. Rev.*, **84**, 139
- Beers T. C., Rossi S., Norris J. E., Ryan S. G., Shefler T., 1999, *AJ*, **117**, 981
- Beers T. C., Norris J. E., Placco V. M., Lee Y. S., Rossi S., Carollo D., Masseron T., 2014, *ApJ*, **794**, 58
- Beers T. C., et al., 2017, *ApJ*, **835**, 81
- Bisterzo S., Gallino R., Straniero O., Cristallo S., Käppeler F., 2010, *MNRAS*, **404**, 1529
- Bonifacio P., et al., 2015, *A&A*, **579**, A28
- Caffau E., et al., 2020, *MNRAS*, **493**, 4677
- Carollo D., et al., 2012, *ApJ*, **744**, 195
- Carollo D., Freeman K., Beers T. C., Placco V. M., Tumlinson J., Martell S. L., 2014, *ApJ*, **788**, 180
- Casagrande L., et al., 2021, *MNRAS*, **507**, 2684
- Chiappini C., Hirschi R., Meynet G., Ekström S., Maeder A., Matteucci F., 2006, *A&A*, **449**, L27
- Chiti A., et al., 2018, *ApJ*, **856**, 142
- Chiti A., Frebel A., Jerjen H., Kim D., Norris J. E., 2020, *ApJ*, **891**, 8
- Christlieb N., Green P. J., Wisotzki L., Reimers D., 2001, *A&A*, **375**, 366
- Christlieb N., Schöreck T., Frebel A., Beers T. C., Wisotzki L., Reimers D., 2008, *A&A*, **484**, 721
- Cohen J. G., et al., 2005, *ApJ*, **633**, L109
- Cohen J. G., Christlieb N., Thompson I., McWilliam A., Shectman S., Reimers D., Wisotzki L., Kirby E., 2013, *ApJ*, **778**, 56
- DESI Collaboration et al., 2016, arXiv e-prints, p. arXiv:1611.00036
- D’Orazi V., Gratton R., Lucatello S., Carretta E., Bragaglia A., Marino A. F., 2010, *ApJ*, **719**, L213
- Da Costa G. S., et al., 2019, *MNRAS*, **489**, 5900
- Dalton G., et al., 2018, in *Proc. SPIE*, p. 107021B, doi:10.1117/12.2312031
- Demarque P., Woo J.-H., Kim Y.-C., Yi S. K., 2004, *ApJS*, **155**, 667
- Frebel A., 2010, *Astronomische Nachrichten*, **331**, 474
- Frebel A., Norris J. E., 2015, *ARA&A*, **53**, 631
- Frebel A., et al., 2006, *ApJ*, **652**, 1585
- Gaia Collaboration et al., 2016, *A&A*, **595**, A1
- Gaia Collaboration Brown A. G. A., Vallenari A., Prusti T., de Bruijne J. H. J., Babusiaux C., Biermann M., 2020, arXiv e-prints, p. arXiv:2012.01533
- Gallagher A. J., Caffau E., Bonifacio P., Ludwig H. G., Steffen M., Homeier D., Plez B., 2017, *A&A*, **598**, L10
- Goswami A., Aoki W., Beers T. C., Christlieb N., Norris J. E., Ryan S. G., Tsangarides S., 2006, *MNRAS*, **372**, 343
- Green G., 2018, *The Journal of Open Source Software*, **3**, 695
- Gustafsson B., Edvardsson B., Eriksson K., Jørgensen U. G., Nordlund Å., Plez B., 2008, *A&A*, **486**, 951
- Hansen T. T., Andersen J., Nordström B., Beers T. C., Placco V. M., Yoon J., Buchhave L. A., 2016a, *A&A*, **586**, A160
- Hansen T. T., Andersen J., Nordström B., Beers T. C., Placco V. M., Yoon J., Buchhave L. A., 2016b, *A&A*, **588**, A3
- Harris C. R., et al., 2020, *Nature*, **585**, 357
- Heger A., Woosley S. E., 2010, *ApJ*, **724**, 341
- Howes L. M., et al., 2014, *MNRAS*, **445**, 4241
- Howes L. M., et al., 2015, *Nature*, **527**, 484
- Howes L. M., et al., 2016, *MNRAS*, **460**, 884
- Hunter J. D., 2007, *Computing In Science & Engineering*, **9**, 90
- Ji A. P., et al., 2020, *ApJ*, **889**, 27
- Keller S. C., et al., 2007, *Publ. Astron. Soc. Australia*, **24**, 1
- Kielty C. L., Venn K. A., Loewen N. B., Shetrone M. D., Placco V. M., Jahandar F., Mészáros S., Martell S. L., 2017, *MNRAS*, **471**, 404
- Koesterke L., Allende Prieto C., Lambert D. L., 2008, *ApJ*, **680**, 764
- Lee Y. S., et al., 2008a, *AJ*, **136**, 2022
- Lee Y. S., et al., 2008b, *AJ*, **136**, 2050
- Lee Y. S., et al., 2013, *AJ*, **146**, 132
- Lee Y. S., Suda T., Beers T. C., Stancliffe R. J., 2014, *ApJ*, **788**, 131
- Lee Y. S., Beers T. C., Kim Y. K., Placco V., Yoon J., Carollo D., Masseron T., Jung J., 2017, *ApJ*, **836**, 91
- Lee Y. S., Beers T. C., Kim Y. K., 2019, *ApJ*, **885**, 102
- Li H. N., et al., 2010, *A&A*, **521**, A10
- Li H., Tan K., Zhao G., 2018, *ApJS*, **238**, 16
- Li H., et al., 2022, arXiv e-prints, p. arXiv:2203.11529
- Limberg G., et al., 2021, *ApJ*, **913**, 11
- Lucatello S., Tsangarides S., Beers T. C., Carretta E., Gratton R. G., Ryan S. G., 2005, *ApJ*, **625**, 825
- Lucatello S., Beers T. C., Christlieb N., Barklem P. S., Rossi S., Marsteller B., Sivarani T., Lee Y. S., 2006, *ApJ*, **652**, L37
- Lucchesi R., et al., 2022, *MNRAS*, **511**, 1004
- Luck R. E., Bond H. E., 1991, *ApJS*, **77**, 515
- Marsteller B., Beers T. C., Rossi S., Christlieb N., Bessell M., Rhee J., 2005, *Nuclear Phys. A*, **758**, 312
- Masseron T., et al., 2014, *A&A*, **571**, A47
- McKinney W., 2010, in Stéfan van der Walt Jarrod Millman eds, *Proceedings of the 9th Python in Science Conference*. pp 56 – 61, doi:10.25080/Majora-92bf1922-00a
- Mészáros S., et al., 2012, *AJ*, **144**, 120
- Meynet G., Ekström S., Maeder A., 2006, *A&A*, **447**, 623
- Nomoto K., Kobayashi C., Tominaga N., 2013, *ARA&A*, **51**, 457
- Norris J. E., Yong D., 2019, *ApJ*, **879**, 37
- Norris J. E., Ryan S. G., Beers T. C., 1997, *ApJ*, **488**, 350
- Norris J. E., et al., 2013a, *ApJ*, **762**, 25
- Norris J. E., et al., 2013b, *ApJ*, **762**, 28
- Placco V. M., et al., 2010, *AJ*, **139**, 1051
- Placco V. M., et al., 2011, *AJ*, **142**, 188
- Placco V. M., Frebel A., Beers T. C., Stancliffe R. J., 2014, *ApJ*, **797**, 21
- Placco V. M., et al., 2018, *AJ*, **155**, 256
- Placco V. M., et al., 2019, *ApJ*, **870**, 122
- Plez B., 2012, *Turbospectrum: Code for spectral synthesis*, *Astrophysics Source Code Library*, record ascl:1205.004 (ascl:1205.004)
- Price-Whelan A. M., et al., 2018, *AJ*, **156**, 123
- Rossi S., Beers T. C., Sneden C., Sevatyanenko T., Rhee J., Marsteller B., 2005, *AJ*, **130**, 2804
- Salvadori S., Skúladóttir Á., Tolstoy E., 2015, *MNRAS*, **454**, 1320
- Schlafly E. F., Finkbeiner D. P., 2011, *ApJ*, **737**, 103
- Schlaufman K. C., Casey A. R., 2014, *ApJ*, **797**, 13
- Schlegel D. J., Finkbeiner D. P., Davis M., 1998, *ApJ*, **500**, 525
- Schöreck T., et al., 2009, *A&A*, **507**, 817
- Shank D., et al., 2021, arXiv e-prints, p. arXiv:2109.08600

- Skrutskie M. F., et al., 2006, [AJ](#), **131**, 1163
- Spite M., Caffau E., Bonifacio P., Spite F., Ludwig H. G., Plez B., Christlieb N., 2013, [A&A](#), **552**, A107
- Starkenburg E., et al., 2013, [A&A](#), **549**, A88
- Starkenburg E., Shetrone M. D., McConnachie A. W., Venn K. A., 2014, [MNRAS](#), **441**, 1217
- Starkenburg E., et al., 2017, [MNRAS](#), **471**, 2587
- Steinmetz M., et al., 2006, [AJ](#), **132**, 1645
- Suda T., et al., 2008, [PASJ](#), **60**, 1159
- Taylor M. B., 2005, in Shopbell P., Britton M., Ebert R., eds, Astronomical Society of the Pacific Conference Series Vol. 347, Astronomical Data Analysis Software and Systems XIV. p. 29
- Tominaga N., Iwamoto N., Nomoto K., 2014, [ApJ](#), **785**, 98
- Umeda H., Nomoto K., 2003, [Nature](#), **422**, 871
- Whitten D. D., et al., 2021, arXiv e-prints, p. [arXiv:2104.00016](#)
- Wolf C., et al., 2018, [Publ. Astron. Soc. Australia](#), **35**, e010
- Yong D., et al., 2013, [ApJ](#), **762**, 27
- Yong D., et al., 2021, [MNRAS](#), **507**, 4102
- Yoon J., et al., 2016, [ApJ](#), **833**, 20
- Yoon J., et al., 2018, [ApJ](#), **861**, 146
- Yoon J., Beers T. C., Tian D., Whitten D. D., 2019, [ApJ](#), **878**, 97
- Yoon J., Whitten D. D., Beers T. C., Lee Y. S., Masseron T., Placco V. M., 2020, [ApJ](#), **894**, 7
- York D. G., et al., 2000, [AJ](#), **120**, 1579
- Yuan Z., et al., 2020, [ApJ](#), **891**, 39
- Zepeda J., Rasmussen K. C., Beers T. C., Placco V. M., Huang Y., Depagne É., 2022, [ApJ](#), **927**, 13
- de Jong R. S., et al., 2019, [The Messenger](#), **175**, 3

Table 1. Compilation of CEMP fractions for halo samples from the literature (samples for dwarf galaxies, globular clusters and stellar streams are not included)

Reference	Sample	Type	LR analysis	Stellar type	[C/Fe] >+1.0 (Beers & Christlieb 2005)					[C/Fe] >+0.7 (Aoki et al. 2007)					evol. cor. ?
					<-3.5	<-3.0	<-2.5	<-2.0	<-1.5	<-3.5	<-3.0	<-2.5	<-2.0	<-1.5	
Norris et al. (1997)	HK	LR	by eye	mix	14										n
Cohen et al. (2005)	HES	LR/HR		giants	14 ± 4										n
Frebel et al. (2006)	HES	LR	Rossi+05	giants	25 ± 11 13 ± 4 9 ± 2										n
Lucatello et al. (2006)	HES	HR		mix	21 ± 2					24 ± 3					n/y (a)
				unevolved	21 ± 5										-
Carollo et al. (2012)	SDSS	LR	SSPP	mix						20 12 8					n (b)
Aoki et al. (2013)	SDSS	HR		giants						36					y (c)
	SDSS	HR		turn-off						>9					-
Yong et al. (2013)	HES+lit	HR		mix	23 ± 6					32 ± 8					y (c)
				dwarfs						50 ± 31					-
				giants						39 ± 11					y (c)
Lee et al. (2013)	SDSS	LR	SSPP	all	41 ± 10	22 ± 3	15 ± 1	8 ± 1	4 ± 1	43 ± 11	28 ± 3	21 ± 1	12 ± 1	8 ± 1	n
				giants						33 ± 11	31 ± 4	32 ± 2	19 ± 1	11 ± 1	n
				dwarfs						100 ± 50	75 ± 22	15 ± 1	3 ± 1	1 ± 1	-
				turn-off						50 ± 29	17 ± 4	10 ± 1	10 ± 1	8 ± 1	-
Placco et al. (2014)	Lit	HR		mix	51	38	28	27		60	48	34	33		y (d)
Beers et al. (2017)	HES	LR	n-SSPP	mix						39 ± 15	24 ± 6	19 ± 4			n (e)
Yoon et al. (2018)	AEGIS	LR	n-SSPP	(sub)giants						78 ⁺⁶ ₋₇	64 ± 3	42 ± 2	26.5 ± 0.8	13.6 ± 0.4	y (d)
Placco et al. (2018)	RAVE	LR	n-SSPP	giants						57 ⁺¹³ ₋₁₄	37	23 ± 3			y (d)
Placco et al. (2019)	RPA/B&B	LR	n-SSPP	giants						47 ⁺²² ₋₂₁	31 ⁺⁹ ₋₇	22 ⁺⁵ ₋₄			y (d)
Limberg et al. (2021)	B&B	LR	n-SSPP	giants						43 ⁺¹⁶ ₋₁₅	32 ± 6	19 ± 3			y (d)
Whitten et al. (2021) (f)	S-PLUS	phot	SSPP-trained	K-dwarfs						60	45	25	20		-
Li et al. (2022)	LAMOST	HR		giants						7.8 ^{+2.2} _{-1.8}					y (c)
				turn-off	11					31 ± 4 (g)					-

Follow-up of VMP candidates from narrow-band photometric surveys

Howes et al. (2016) (h)	SkyMapper	HR		giants (bulge)						44 ⁺¹⁶ ₋₁₅	18 ⁺¹⁰ ₋₇	20 ⁺⁸ ₋₆			y (d)
Aguado et al. (2019) (i)	Pristine	LR	FERRE	turn-off						41 ⁺¹² ₋₁₁					-
				giants						38 ⁺¹⁸ ₋₁₅					n (b)
Caffau et al. (2020)	Pristine	LR	MyGIsFOS	mix						31 ⁺¹⁴ ₋₁₁					n
Arentsen et al. (2021)	PIGS	LR	FERRE	giants (bulge)						17 ⁺⁷ ₋₅					y (d)
Lucchesi et al. (2022)	Pristine	HR		unevolved						41.7 ^{+14.3} _{-13.0}					-
				giants						16.4 ^{+3.0} _{-2.6}					n
Yong et al. (2021) (j)	SkyMapper	HR		mix						60 ⁺¹⁰ ₋₁₁					y (d)
										11 ⁺¹⁰ ₋₅					-
										20 ⁺⁴ ₋₄					y (d)

In general, if the absolute numbers of stars were given in a paper, we estimated uncertainties using binomial statistics.

(a) no for 1.0, yes for 0.7 using the Aoki et al. (2007) luminosity definition (b) but few evolved stars (c) using the Aoki et al. (2007) luminosity definition (d) using the P14 corrections (e) if P14 corrections are applied the number of CEMP stars goes up from 52 to 57 (f) estimated from their Figure 13 (g) the lower limit is 22 ± 3 %, assuming all stars without detected CH bands are not carbon-enhanced (h) as updated in Arentsen et al. (2021) (i) as updated in this work, see Section 2.3 (j) computed from their published table, only taking into account stars without upper limits on [C/Fe]

APPENDIX A: CROSS-ANALYSIS OF THE FERRE AND SSPP SYNTHETIC GRIDS

The systematic differences in $[C/Fe]$ between the (n-)SSPP and FERRE analyses (even when the other stellar parameters are consistent) could come from different approaches to deriving carbon abundances in these codes, and/or from the use of different synthetic grids. FERRE fits the full spectrum and uses a running mean normalisation, whereas the (n-)SSPP only fits a small region in the G-band (between 4290 – 4318 Å) and normalises using a pseudo-continuum determined over the 4000 – 4650 Å range. The synthetic grids have different assumptions (see Section 3.2), those that are most likely to cause discrepancies in the derived $[C/Fe]$ are the adopted line lists for carbon features, the adopted nitrogen abundances, and possibly the difference in adopted micro-turbulence velocities.

A preliminary look at the line lists shows that there do appear to be differences in the strengths of the CH lines between the Kurucz and Masseron line lists, with the Kurucz lines being stronger (M. Montelius, private communication). Regarding the assumptions on nitrogen abundances, they do not only have a direct effect on the CN features, but also indirectly affect e.g. the G-band and other CH/C₂ features due to the contribution of nitrogen to the overall metallicity of the stellar atmosphere. It is beyond the scope of this work, which is focused on the observations, to investigate detailed differences in the synthetic grids. Instead, we investigate the effects of adopting different grids and/or analysis methods for the derivation of $[C/Fe]$.

We performed a cross-analysis of the two synthetic grids: we analysed spectra from the SSPP grid with FERRE, and spectra from the FERRE grid with the n-SSPP. When fitting the SSPP spectra with FERRE, we keep T_{eff} , $\log g$ and $[Fe/H]$ fixed to the true values from the SSPP grid, and only fit for $[C/Fe]$. We fit the spectra between 3900 – 5500 Å. When running the n-SSPP carbon routine on the FERRE spectra, we keep T_{eff} and $\log g$ fixed to the true values from the FERRE grid, deriving $[C/H]$. Both grids were smoothed to $R = 1000$, which is the resolution used in the n-SSPP.

The results are shown in Figure C1, with on the left-hand side the FERRE analysis of the SSPP grid and on the right-hand side the n-SSPP analysis of the FERRE grid, separated by $[Fe/H]$ in different panels and colour-coded by T_{eff} . For $[C/Fe] < +1.5$, the average difference (combining all T_{eff}) is close to zero for all metallicities, but there are systematics that vary with the effective temperature, of the order of ~ 0.1 – 0.2 dex. The effect is similar in both analyses: the cool stars typically have higher FERRE $[C/Fe]$ and the warmer stars typically have lower FERRE $[C/Fe]$. This appears to be a characteristic of the synthetic grids. However, the magnitude of this effect is larger in the n-SSPP analysis, possibly because it is fitting a much smaller wavelength range.

For the very carbon-rich stars with $[C/Fe] > +1.5$, other systematics start to appear, especially for the more metal-rich cases ($[Fe/H] = -2.0$ and -2.5). In the n-SSPP grid, the very carbon-rich stars are also strongly enhanced in nitrogen ($[C/Fe] = [N/Fe]$), whereas the in the FERRE grid nitrogen is fixed with respect to iron ($[N/Fe] = 0$). This results in large differences in the spectra, which the different approaches of the n-SSPP and FERRE appear to respond to differently. For very carbon-rich stars, the different normalisation schemes may also introduce differences in the derived $[C/Fe]$.

APPENDIX B: PHOTOMETRIC TEMPERATURES

The FERRE T_{eff} showed a systematic offset compared to the SSPP T_{eff} values for the coolest stars in the SDSS and LAMOST samples.

Here we compute photometric temperatures and compare them to the spectroscopic values to identify which of the two analyses is at the root of this offset. To compute photometric T_{eff} estimates, we use the photometric temperature relation from Casagrande et al. (2021) applied to *Gaia* EDR3 (BP–RP) photometry (Gaia Collaboration et al. 2016, 2020), which includes terms that depend on $\log g$ and $[Fe/H]$. The $\log g$ dependence is small, and we adopt $\log g = 2.0$ for all stars. For $[Fe/H]$ we adopt the SSPP values, but changing to the FERRE values does not affect the results. We deredden the photometry adopting $E(B-V)$ values from the Schlegel extinction map (Schlegel et al. 1998; Schlafly & Finkbeiner 2011), using the colour-dependent extinction coefficients for the BP and RP photometry from Casagrande et al. (2021). The resulting comparison between spectroscopic and photometric effective temperatures is shown in Figure C2, for the SDSS sample on the left and the LAMOST sample on the right, with the SSPP results in red and the FERRE results in blue. The issue with the cool stars appears to be an issue in the FERRE analysis, as the same systematic offset is visible.

This bias was very puzzling at first, because it is not seen for the RAVE/NTT spectra where the T_{eff} is well-determined even for the coolest stars. We then checked the metallicities for the $T_{\text{eff}} < 5000$ K stars in the different samples, and found that in this temperature range, the SDSS and LAMOST stars are clearly more metal-poor than those in the NTT sample. The more metal-poor a star is, the fewer spectral lines are present, and the harder it is to estimate T_{eff} and $\log g$ from spectra alone. This is particularly the case for the coolest stars (e.g. $T_{\text{eff}} < 5000$ K), where the $T_{\text{eff}}/\log g$ -sensitive Balmer lines become very weak. Many of the spectral lines in VMP stars are in the bluest part of the spectrum, and an additional disadvantage of the SDSS spectra is that they do not go bluer than 3820 Å.

The FERRE analysis is purely spectroscopic, whereas the SSPP analyses also include photometry in the stellar atmospheric parameter determination. This is likely the reason that the FERRE T_{eff} determinations for cool, very metal-poor stars are less good than the SSPP determinations.

We finally note that the systematic behaviour between the spectroscopic and photometric temperatures is the same for both FERRE analyses of the SDSS and LAMOST spectra, but that it is different for the two SSPP analyses. The scatter in the photometric vs. SSPP T_{eff} also increases for the LAMOST sample. We already saw larger discrepancies between the other stellar parameters ($\log g$, $[Fe/H]$) in the FERRE and SSPP analyses of the LAMOST spectra (see the left-hand column of Figure 5). These may be indications of larger systematic issues in the n-SSPP.

APPENDIX C: CROSS-COMPARISON OF THE PARAMETERS FROM FERRE AND N-SSPP

We present parameter differences between for two parameters between our FERRE and n-SSPP analyses of the LAMOST, SDSS, RAVE and PIGS samples in Figure C3. This comparison allows to recognise degeneracies between various parameters. The top row shows the well-known correlation between $[Fe/H]$ and T_{eff} for low-resolution spectroscopic analyses of metal-poor stars. There also appears to be a slight degeneracy between T_{eff} and $[C/Fe]$. The other rows, presenting the difference in $[C/Fe]$ versus differences in $[Fe/H]$ and $\log g$, show no strong degeneracies.

This paper has been typeset from a \LaTeX file prepared by the author.

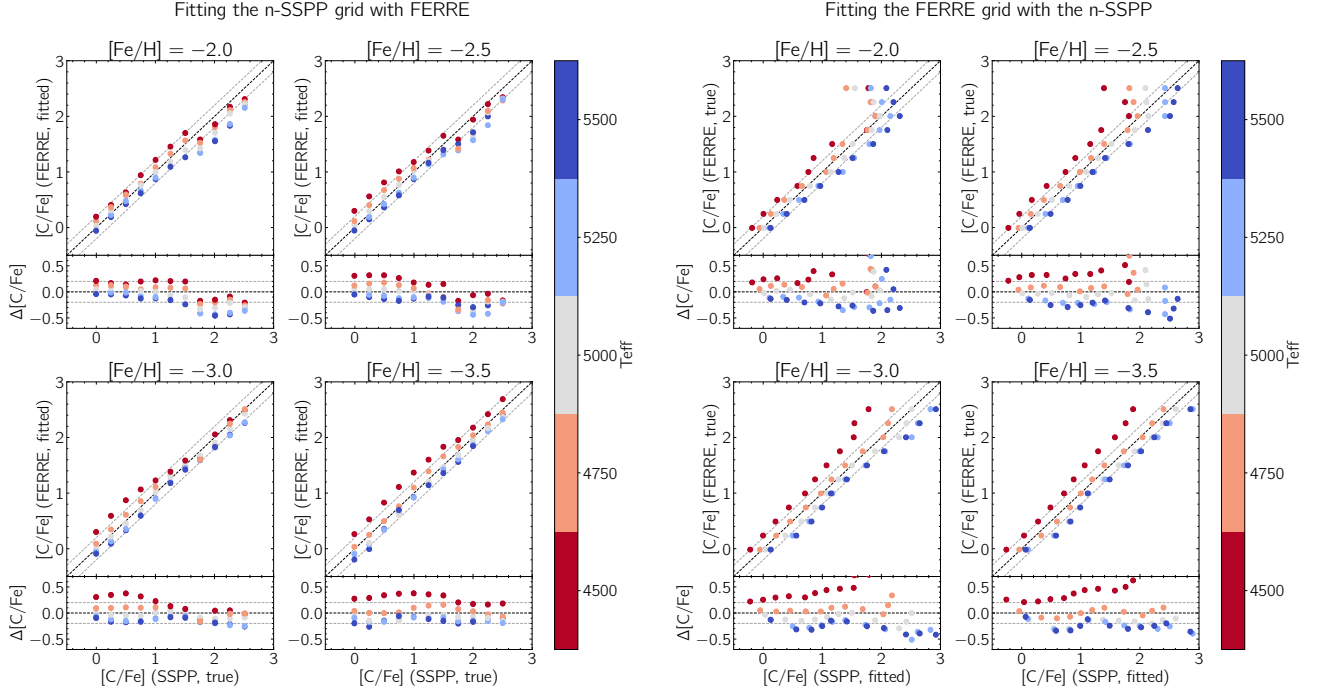


Figure C1. Results of the cross-analysis of the FERRE and n-SSPP synthetic grids as function of $[C/Fe]$, $[Fe/H]$ (different panels) and T_{eff} (colour). The left-hand side shows the results of the n-SSPP analysis of the FERRE grid, the right-hand side the FERRE analysis of the n-SSPP grid. The black-dashed line is the one-to-one line, the grey-dashed lines are ± 0.2 dex. The $\Delta[C/Fe]$ in the bottom panels is always FERRE – SSPP.

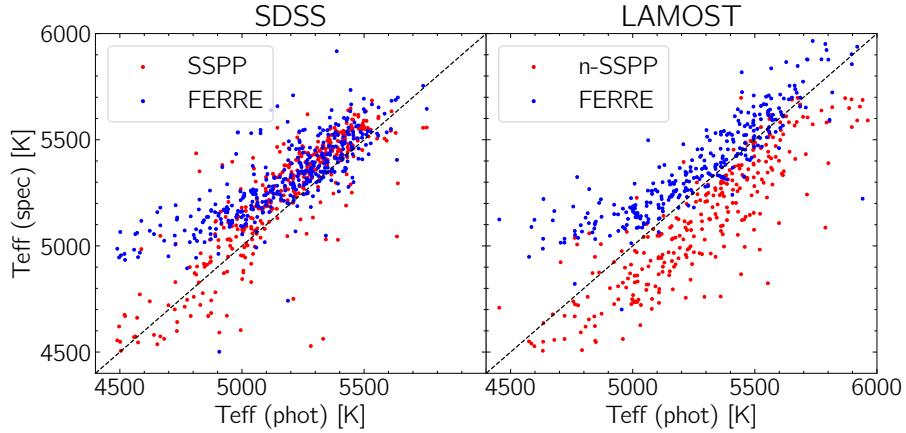


Figure C2. Comparison of spectroscopic and photometric effective temperatures for the (n-)SSPP and FERRE analyses of the SDSS and LAMOST samples.

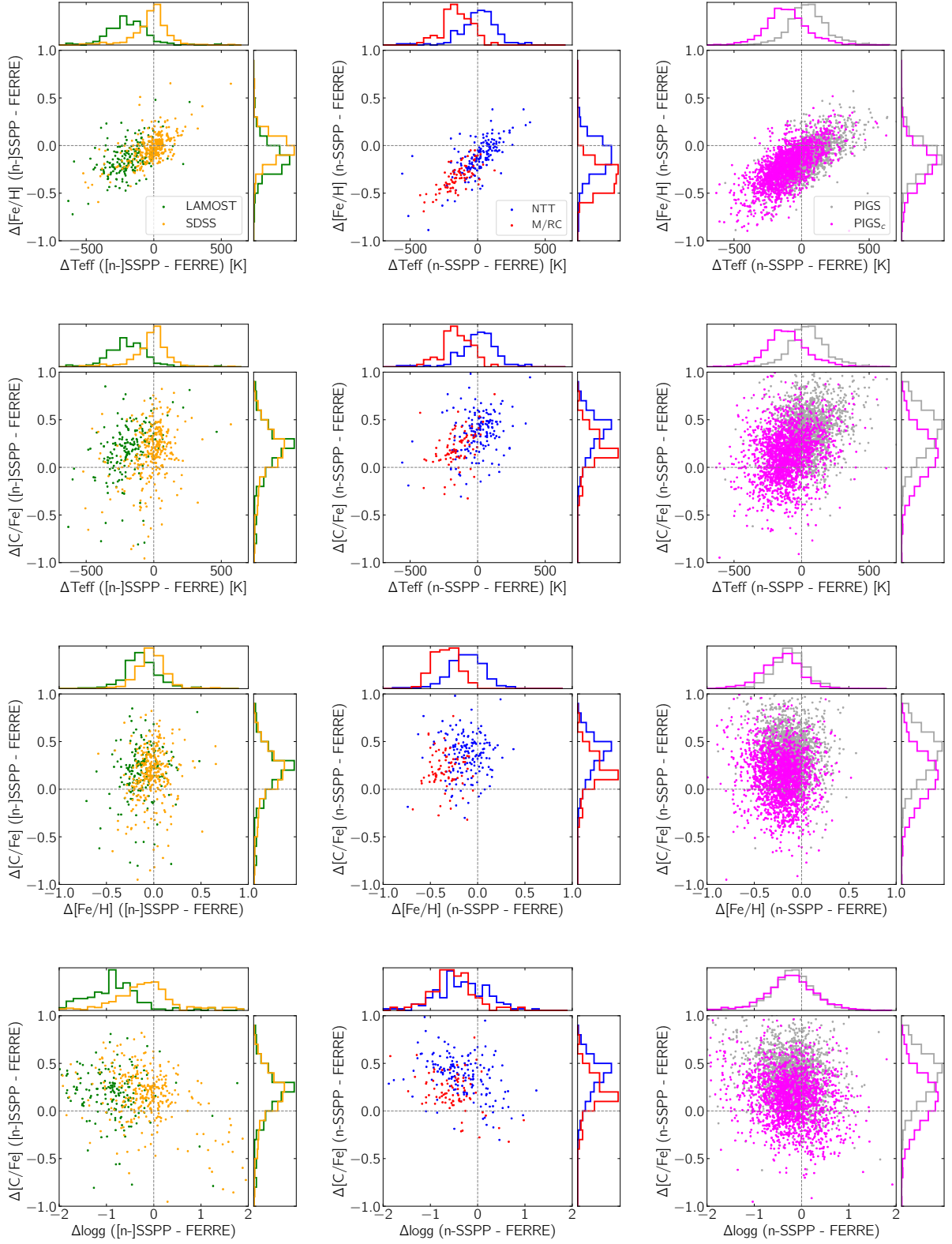


Figure C3. As in Figure 5, but comparing the differences between two parameters. For the SDSS/LAMOST panels, only stars with (n-)SSPP $T_{\text{eff}} > 5000$ K have been included.